Final Report

Anchorage Pour-backs Durability

Anthony Addai Boateng and Natassia Brenkus

The Ohio State University

July 2023

Acknowledgments

We wholly appreciate the financial support of The ACI Foundation which provided the funding for this work.

The contents of this report reflect the views of the authors, not the American Concrete Institute nor the ACI Foundation.

.

Contents

List of Figures and Tables

INTRODUCTION

1.1 Problem Statement

Pour-backs at post-tensioning (PT) tendons anchorage ends provide corrosion protection to the anchorage hardware, improving the durability of post-tensioned structures. However, the interface may serve as a pathway if deficiencies are present between the PT structure and the pour-back material, providing a route for water and other factors that could negatively affect the structure's integrity. Therefore, this research addressed the need to develop a pour-back material guidance and test methods to improve the bond at the interface. When a pour-back is not detailed at the anchorage regions, the exposure to corrosive agents causes failure of the tendons because of corrosion of the strand in the anchorage. Figure 1 presents post-tension failure on Podium Deck, Sunshine Coast resort, because of corroded post-tensioning tendons.

Figure 1: Post-Tensioning Failures on Podium Deck, Sunshine Coast Resort

1.2 Research Background

This research aimed to investigate the traditional practices associated with pour-back construction considering the commonly specified constitutive materials and the types of surface preparations and to investigate existing construction methods' influence on the integrity of pour-backs. This work aims to suggest improvements to construction and testing approaches. The surface preparation methods were evaluated by mechanical testing (bond strength), microstructural analysis (porosity determination), chloride permeability, and ultrasonic pulse velocity (UPV).

A recent study compiles the published current anchorage pour-back standards and specifications used by some state agencies represented in Table 1 (Tatum et al., 2021). These standards are generally recognized as the current best practices for anchorage protection.

Table 1. Current Anchorage Pour-back Specifications (Tatum and Brenkus 2021)

Agency	Specs	Last updated	Pour-back material	Surface Preparation method
Florida DOT	Standard Specifications for Road and Bridge Construction 462-7.3.3.2	11/1/2018	Reinforced concrete, magnesium ammonium phosphate concrete, or a Type Q Epoxy grout	Grit or water blasting
California DOT	Standard Plan B8-5 Standard Specification 50-1.03B(2)©	1/29/2018	Same as concrete structure	None specified
Ohio DOT	Supplemental Specification 855.17	4/20/2018	Epoxy grout	Grist water blasting at 10,000 psi nozzle pressure with a minimum pull-off of 175 psi
PTI	M50.3-12 Section 14-2	9/1/2019	Concrete or Epoxy grout	Grit or water blasting at 3,000 psi nozzle pressure with minimum pull-off of 175 psi

LITERATURE REVIEW

Several research activities have investigated corrosion agents' ability to penetrate to the anchorage of post-tensioned (PT) structures (Hartt, 2018; Miller et al., 2017). The protection of post-tensioned anchorages is essential for durable PT structures. By so doing, the strands under tensile force are protected, increasing the structure's life span. The PT anchorage comprises three layers, which protect the strands from corrosion (Tatum et al., 2021), a permanent grout, a plastic cap, and a pour-back material. In this way of protection, the tendons are safe from corrosion agents.

The testing and grouting approaches intended in this research activity consider the influence of voids, hypothesizing that high permeability and defects at the pour-back interface could serve as the pathway for the main agents needed to initiate corrosion activities within the structure.

Several researchers have investigated the relationship between porosity and permeability of concrete. Permeability measures the rate of fluid transfer under a pressure gradient – which may be related to the void structure, while porosity directly measures the volume of voids, whether or not they participate in fluid transfer. The permeability of concrete is a good indicator of concrete durability by directly and indirectly describing aggressive agents' infiltration rate (Choinska et al., 2007). If pores are interconnected with high porosity, permeability is high. If pores are high in quantity but disconnected, porosity is considered high but low permeability (Kearsley & Wainwright, 2001). Entrained air and the resultant air voids generally improve workability during placement and increase structural durability. The air void in concrete is categorized based on the size criteria as entrapped or entrained. Sufficient effort is required to prevent the entrapped air voids from exceeding a certain threshold since they negatively affect the strength and durability of a structure. Though air entrained secures frost resistance in concrete, it also increases porosity (Chen et al., 2021). These links between air voids and durability call for porosity investigation at the interface between the concrete substrate and the pour-back.

Chloride Ion Analysis

Chloride ion penetration and contamination are known instigators of PT tendon corrosion. Chloride ions may exist in the original mix before casting or infiltrating a concrete structure from the external environment. Several instances of substantial corrosion in jetty substructures have occurred due to chloride contamination in marine environments (Liam et al., 1992). Figure 2 illustrates the effects of tendon corrosion due to chloride ions.

Diffusion is the movement of molecules from a region of higher concentration to a lower concentration region. Employing a plastic cap cover over the anchorage prevents the diffusion of chlorides as it serves as a physical barrier at this one location (Tatum et al., 2021). Chloride migration coefficient in cement-based material is more sensitive to the change of porosity as He et al. (2019) concluded.

The role of chloride ions on the service of life of concrete structures have been widely investigated into (Angst et al., 2009; Martín-Pérez et al., 2000). Reducing or avoiding the access of chloride and limiting the initial chloride content throughout the service life of a structure is critical in mitigating chloride-induced corrosion problems (Bolzoni et al., 2022). Therefore, understanding

how the chloride ions diffuse through pour-back can offer a better estimation of the service life of the pour-back (Tatum et al., 2021). The chloride limits for prestressed concrete is 0.08 percent acid-soluble chlorides by weight of cement (ACI-222.2R-01).

Image courtesy (Whitmore & Eng, n.d.)

Figure 2. Observed active corrosion of strands

Ultrasonic Pulse Velocity

Several researchers have investigated the relationships between ultrasonic pulse velocity (UPV) and other properties of cementitious materials, such as tensile strength, modulus of elasticity, porosity, among others. UPV is a widely-used, non-destructive test (NDT) which is sometimes used to assess the integrity of structures. This test is grounded on measuring how long an ultrasonic wave takes to pass through a concrete material specimen and determining the wave velocity depending on the length of the specimen. A surface crack depth can be measured using the UPV (ACI-228.2R-1998). A change detected in the wave travelling time and the calculated wave velocity may indicate a presence of defect in the specimen. The intention of performing the UPV as part of this research is to determine the transit time through the interface between the substrate and the overlay. It is hypothesized that defects in the interface may be interpretable in the UPV data.

UPV Working Principle

When an impact affects a concrete surface of a specimen, ultrasonic waves are produced. These waves propagate through the specimen parallel to the sound traveling through the air. The testing equipment consists of a high-voltage pulser, an amplifier, and a detection unit, which includes a synchronized electronic timer, a transmitter, and a receiver. The piezoelectric transducers generate ultrasonic stress waves; the receivers detect the propagating waves. Typical transducers generate the ultrasonic waves in an average ranging from 20 kHz to 300 kHz for concrete applications. For the purposes of this research, the average frequency considered was 50 kHz. Specific detail of this methodology is described in Karaiskos et al. (2015).

Methods of Testing

There are three methods of performing the UPV test, delineated by the wave transmission or the direction of the wave propagation relative to the detector.

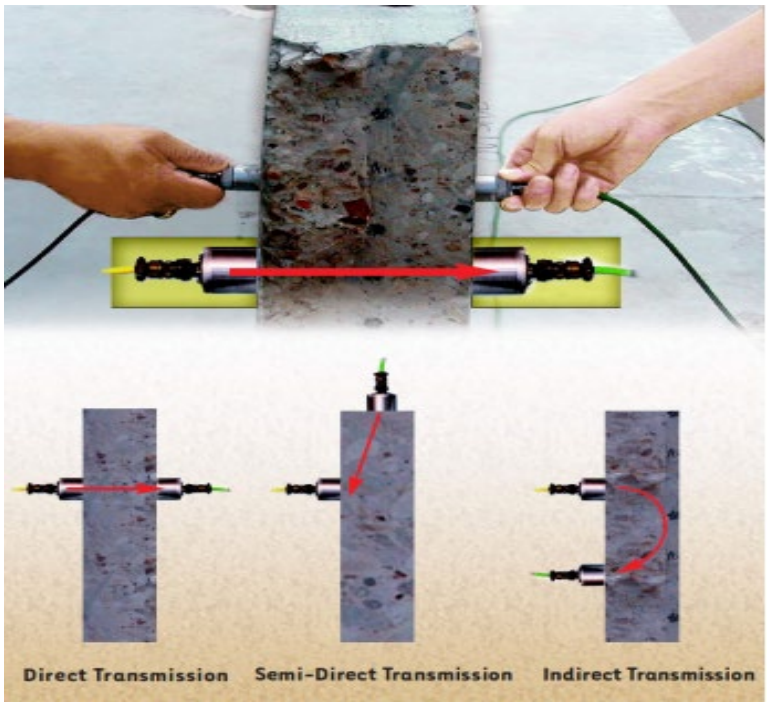

Image courtesy of Olson Engineering

Figure 3. UPV Methods of testing

The transmission method influences the sensitivity. Direct transmission is the most sensitive test method, followed by semi-direct; indirect transmission is the least sensitive. Direct and semi-direct transmission were utilized for the prisms and cylinders in this research activity (Figure 3). The semi-direct transmission method was conducted on the prism specimens, and the direct transmission on the cylindrical specimens.

Microstructure Analysis by Scanning Electron Microscopy

Microstructural analysis using scanning electron microscopy (SEM) imaging provides detailed images of a concrete specimen's microstructure. SEM can produce quality images of the microstructure, and the high spatial resolution of the images. Scrivener et al. (Scrivener et al., 1986) investigated the concrete microstructure using SEM; images obtained were analyzed to quantify the microstructural features of the concrete. Although the application techniques of SEM in concrete and cementitious studies have increased in recent years, its use is relatively unknown to many practicing engineers in the concrete industry.

Application methods of SEM for analyzing the microstructure of concrete and cementitious materials to determine the porosity at various scales using backscattering scanning electron (BSE) microscopy have been the focus of much research (Tsakiroglou et al., 2009). The BSE imaging

method can distinguish the phases, such as aggregates, pores, hydrated cement paste, anhydrous cement paste, interfacial transition zone (ITZ), and cracks of a polished specimen.

RESEARCH METHODOLOGY

3.1 Introduction

A comprehensive experimental program was designed to evaluate pour-back characteristics with a known correlation to durability. The research activity considered both different types of surface preparations and pour-back materials. The following experimental methodologies were utilized to investigate the quantifiable characteristics of interface regions:

i. Chloride ion permeability,
ii. Pull-off strength, and
iii. Ultrasonic Pulse Velocity (UPV)
iv. Microstructural analysis (porosity determination).

3.2 Experimental Groups

The surface preparations for this research activity were 1) wet-sand-blast with a 3,000-psi pressure washer, 2) water blasting with a 3,000-psi pressure, and 3) no surface preparation.

Two types of constitutive pour-back material were considered: BASF's Masterflow 648 high-strength high-flow epoxy (Epoxy Grout) and Master Builders' Masterflow 928 low-dust, high-precision mineral aggregate grout (Cementitious Grout). The table below presents the experimental groups (Table 2). A concrete mix conforming to Ohio Department of Transportation QC2 specifications was utilized for all concrete substrates. Two pour-back materials were utilized: epoxy grout and non-shrink proprietary cementitious grout.

Table 2. Experimental Groups

Pour-back Material	Surface Preparation Procedure		
	Wet Sand Blasting with a 3,000-psi nozzle	Water Blasting with a 3,000-psi nozzle	No preparation
Cementitious Grout	CGSB	CGWB	CGN
Epoxy Grout	EGSB	EGWB	EGN

3.2.1 Surface Preparation Procedures

The surface preparation was achieved with a commercially-available pressure washer rated for a maximum pressure of 3,300 psi. Water and wet sandblasting were performed using a 15° spray nozzle (Figure 4). In performing the water jetting, a 3-4 inches distance from the surface of the concrete slab to the tip of the nozzle was used to achieve a surface roughness of approximately ¾". For this method, four passes were conducted to achieve a uniform coarse aggregate exposure. This water blasting method was achieved at 0.004 in^2/s to expose the coarse aggregate properly.

Subsequently, the wet sandblasting procedure had a rate of 0.02 in^2/s to expose the coarse aggregate. The cylindrical and prism specimens also had the same rate as the concrete slab to achieve the coarse aggregate exposure at the surface appropriately.

The wet sandblasting was performed at the same distance (3-4 inches) as the water jetted from the concrete slab's surface to the nozzle's tip. A ceramic sandblasting nozzle and specially graded clean sand was used for the sandblasting.

Figure 4. A 15° pressure washer spray tip

All the prepared surfaces were ponded with water for 48 hours. The surfaces were maintained in a saturated surface dry condition. Efforts were made for the surface to be clean from dirt and other contaminants that could impede the bond of the overlay. Figure 5 represents the surface preparation methods performed on all test samples. Samples ready for grout are shown in Figure 6.

(a)

(b)

(c) (d)

Figure 5. (a) Water blasting on slab, (b) Sand blasting on slab, (c) Water blasting on prisms and cylinders, and (d) Sand blasting on prisms and cylinders

(a) (b)

Figure 6. (a) Passed illustrated surface preparation for slab. 1-sand blast, 2-water blast, and 3- no preparation; (b) Prism and Cylinder specimens ready for grouting

3.2.2 Compression Test

Compression tests were performed at 28-days and 90-days per the ASTM C39 standard (Figure 7c). Table 3 represents the specimens' parameters. During the test, a 4-inch steel retainer with unbounded capping neoprene pads were employed at the ends of the cylinder specimens to ensure parallel, uniform bearing surfaces perpendicular to the applied axial load during the testing (Figure 7a).

Table 3. Specimens Parameters

Specimens	Dimensions (Height x Diameter) inches	Weight (lbs.)
1	7.875x4	8.208
2	8.125x4	8.431
3	8.188x4	8.556

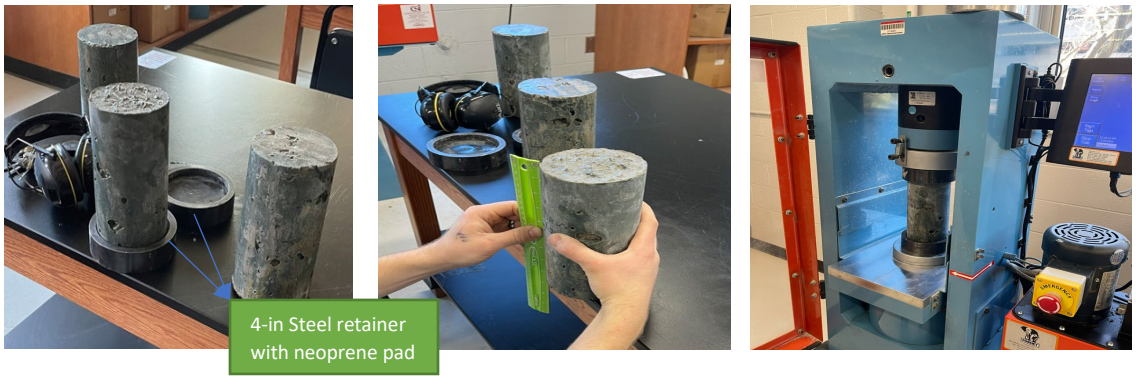

(a) *(b)* *(c)*

Figure 7. (a) Compression test specimens, (b) Measuring the test specimens, (c) Specimen in compression test equipment

For the pour-back materials, a compression test performed on the 2 in. x 2 in. was in accordance with ASTM C109 (Figure 8a and b). The test was conducted to confirm the compressive strength of the grout provided by the manufacturer.

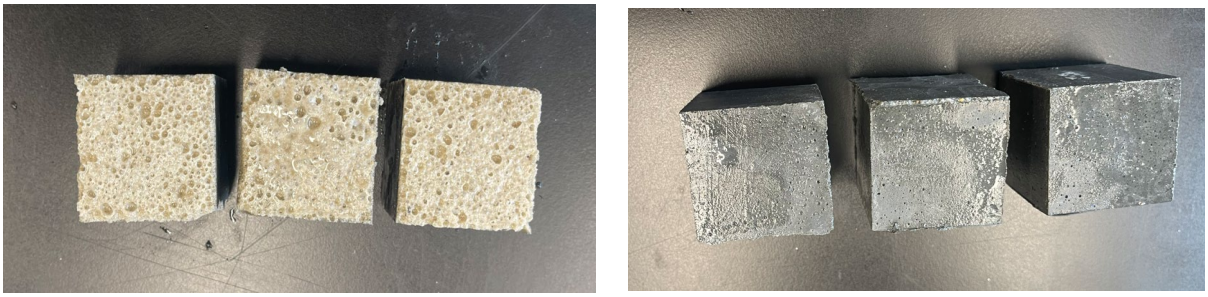

(a) *(b)*

(c)

Figure 8. Compression test specimens (a) Epoxy grout specimens, (b) Cementitious grout specimens, (c) Specimen in compression test equipment

3.2.3 Grouting Process

A secondary pour was performed to apply the selected pour-back materials to the substrate. The same process was conducted for prism, cylinder, and slab specimens.

All specimen surfaces were clean and free of dust, dirt and curing components before placing the grout. The cementitious grout (eight bags) was mixed with the recommended minimum amount of water, 12 pounds (lbs.) for three minutes to ensure uniformity of the mixed product. The cementitious grout was then transferred to a wheelbarrow and scooped into all test forms and molds. The laboratory temperature at the time of casting was approximately 68 ºF.

(a) *(b)*

Figure 9. (a) Mixing the two liquid components of the epoxy grout, (b) Cementitious Grout

The epoxy grout was mixed following the manufacturer's recommendations. The two liquid components were stirred thoroughly to form a compound and poured into the mixer; the last component, the sand, was then added and mixed in for the recommended mixing time.

(a) (b) (c)

Figure 10. (a) Concrete slab with Cementitious Grout, (b) Concrete slab with Epoxy Grout, and (c) Prism and Cylinder samples with grout

(a) (b) (c)

Figure 11. (a) Concrete Substrate and Epoxy grout with (1) Wet Sand surface preparation, (2) Water jetting surface preparation, and (3) No surface preparation; (b) Concrete Substrate and Cementitious grout with (4) No surface preparation, (5) Water jetting, and (6) Wet Sand surface preparation.

Figure 11(a) presents the demolded concrete-epoxy grout halves prism specimens, which measures 6 in. x 6 in. x 10.5 in. The prisms were all considered for the ultrasonic pulse velocity test (UPV). Specimens 1, 2, and 3 had no preparation, water jetting, and wet sand blasting surface preparation, respectively. None of the concrete epoxy grout prism specimens experienced separation after the demolding process.

Figure 11(b) shows the concrete-cementitious grout prism specimens. Specimens 4, 5, and 6 had no preparation, water jetting, and wet sandblasting surface preparation, respectively. Specimens 4 and 5 - prepared with water jetting and no preparation, respectively - separated as they were demolded. The separation may be hypothesized to be due to a weak cohesive bond between the concrete substrate and grout. Meanwhile, the concrete-cementitious grout specimen with the wet sand surface preparation (specimen 6) provided a substantial cohesive bond between the concrete substrate and grout.

Figure 11(c) presents different sizes of cylindrical specimens, a 4 in. x 8 in. half filled with grout and the other half with concrete, which is used for the UPV test, 6 in. x 12 in. half filled with

concrete and the other, with concrete was used for chloride profiling test, and a 4 in. x 8 in. full concrete, considered for compression and modulus of elasticity (MOE) test.

3.2.4 Mechanical Testing (Bond Strength Test)

The bond strength test is a direct method described by ASTM C1583 (ASTM C1583) test method (Standard Test Method for Tensile Strength of Concrete Surfaces and the Bond Strength or Tensile Strength of Concrete Repair and Overlay Materials by Pull-off Method) for concrete-grout slab. In performing the test, an epoxy glue was attached to a 2-inch diameter steel disk (dolly) on top of the cored location (Figure 17a). The test was performed after 24 hours of gluing the steel disk. A tensile load was then applied until failure occurred. The failure load and mode were recorded. According to the ASTM C1583, at least three valid tests should be done and the results averaged for the exact failure mode.

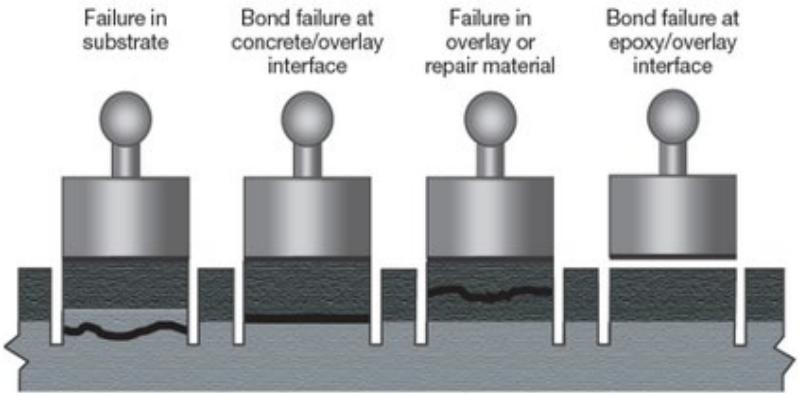

Image courtesy of Papworths Construction Testing Equipment

Figure 12. Direct tension test failure modes

Figure 12 presents the types of tensile failures that can occur during the bond strength test. A tensile failure in any constitutive material indicates that the bond at the interface is stronger than the tensile strength of both the concrete and the overlay; this is a desirable outcome, though it cannot reveal the full strength of the bond, specifically. The failure along the interface characterizes the bond strength.

For the pull-off strength test, wood forms were built from 4 in. x 8 in. plywood and a 4 in. x 8 in. wood to cast the slab. The concrete slabs were constructed such that the coring rig could be directly mounted to the face of the slab to eliminate differential movement between the test site and the coring rig. Plywood formed the bottom and side of the formwork, and the 2x4 as assembly with L-brackets at the outside corners of the formwork to hold the plywood together. The inside of the form measured 54 in. x 39 in., and the outside measured 58.4 in. x 40.4 in. A 4 in. x 4 in. pressure-treated lumber and a 1 in. x 4 in. deck boards were used to construct a pallet to support the formwork. These pallets were placed to prevent stress concentration in the concrete slab during transport around the lab.

After building the formwork, all corners and joints were sealed with silicone caulk. Rebar was placed at the bottom of the concrete to control cracking during the vibration of the concrete slab

during coring and tie in vertical anchors for the coring machine. The reinforcement was spaced so it would not interfere with harvesting the coring specimens.

To perform coring, the drilling rig was attached to the concrete surface with an anchor, bolt, or vacuum seal to stabilize the rig. A 3/8 in. diameter threaded rod was attached to the rebar at equal spacing to serve as an anchor. The rods were placed before casting the slab.

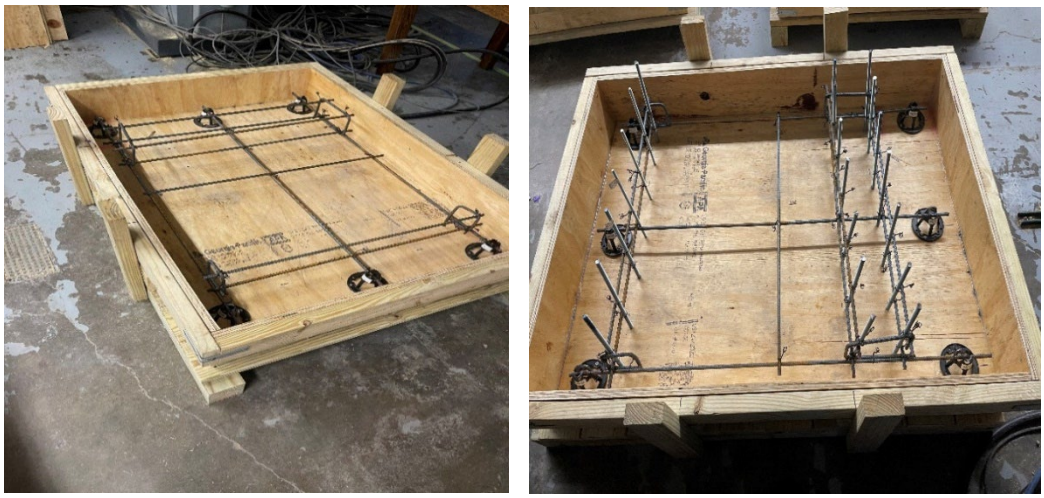

(a) *(b)*

Figure 13. (a) and (b) Wood formwork with No. 3 rebar and 3/8" threaded rod

Figure 14. Forms ready for concrete casting

The concrete used for this work was batched by a local readymix supplier and delivered to the OSU Civil Engineering laboratory. The weather at the time of the concrete delivery was 39° F, with humidity of 59%. Before casting all the test specimens, a slump test was conducted to assess workability. The concrete had a slump of 4" upon delivery.

All specimens were batched by discharging concrete into wheelbarrows, shoveling, and troweling into forms. Slab specimens were compacted with a vibratory compactor. The specimen surfaces were smoothed and leveled with a trowel. The specimens were covered with plastic allowed

allowed to set for 24 hours. Following setting of concrete, all the slab specimens were covered with wet burlap and cured at a temperature of 68 ºF.

(a) *(b)*

Figure 15. (a) and (b) Concrete Slab

The size of the pull-off test slab measures 54-inch by 39-inch with a concrete substrate thickness of 5-inch and a 2-inch thick of the grout overlay. The pull-off test was conducted when the concrete substrate was 90-days old, and the grout overlay was 60-days old. The locations of the test surfaces were grounded with an angle grinder to guarantee a smooth surface. The dollies were attached to the cored sites using a Sikadur Hi-Mod epoxy. The epoxy was allowed to cure for 24-hours prior to pull-off testing. A tensile load was applied using Elcometer 510 adhesion tester, and the failure modes were recorded (Figure 17). Figure 16 presents the pull-off test techniques and problems encountered. The slabs were relatively big enough such that the mass of concrete dampened the vibrations.

(a) *(b)*

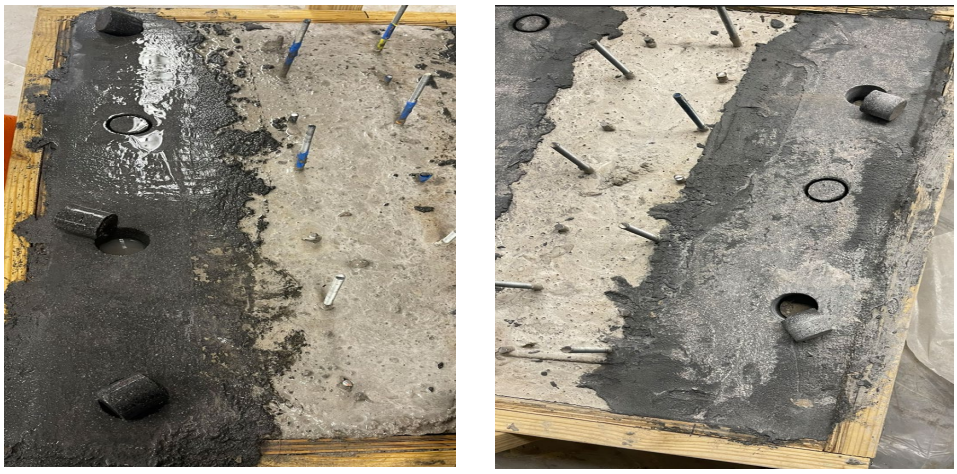

(c) *(d)*

Figure 16. (a) During Coring, (b) After coring, (c) and (d) Broken cores

(a) *(b)*

Figure 17. (a) Steel disks glued to the surfaces of cored locations, (b) Pull-off testing

3.2.5 Ion Permeability Testing

Concrete structural durability depends on the environmental surroundings and exposure conditions (Sakr, 2005). These factors influence mecahnisms of freeze and thaw, corrosion, alkali-silica reaction, carbonation, and transport mechanisms, such as absorption and diffusion. Many test methods and techniques have been developed to evaluate the link between chloride ion permeability and a concrete structure's corrosion resistance. Steel corrosion in reinforced concrete structures has a massive effect on its durability, causing untimely physical deterioration of the structure and potentially leading to structural failure (Elsener, 2005). The test methods include electrically-induced migration test which involves the usage of an electrical current to drive ions through a concrete sample ((NordTest 355, 1997, and NordTest 492,1999), the evaluation of concrete sample against the penetration of aggressive agents based on the flow of electrical current, which is the electrical resistivity (Ghosh, n.d.; Konečný et al., 2017), the determination of concrete electrical resistivity parameter takes minutes, and the duration of the test is extremely fast

compared to chloride penetration test (NT Build 443, 1995), chloride profiling technique measures the natural diffusion of chloride ions through a concrete sample by dissolving chlorides in solution and adding silver nitrate to perform an equivalence point analysis (Burris & Riding, 2014; Song et al., 2008, ASTM C1152 and ASTM C1556)

To define the permeability of ions along the concrete-grout interface of PT pour-backs, chloride profiling was performed to measure chloride ion diffusion. The testing was conducted in accordance with ASTM C1152 and ASTM C1156. ASTM C1152 details the procedure for calculating the acid-soluble chloride content and ASTM C1156 outlines the sampling protocol for building a chloride diffusion profile.

3.2.5.1 Specimen Preparation

Samples for the ion permeability testing were prepared per ASTM C1556 except a 6-inch by 12-inch cylinder was used instead to ensure enough material could be milled at the interface site to perform the test. The concrete was first cast in one-half plastic cylinder mold. The specimens were set and demolded at 24-hours after casting. The specimens were kept in a fog room for moist curing. After 28 days, surface preparation was conducted on the half-face of the cylindrical specimens.

Surface preparation was conducted 48 hours prior to the casting of the grout. Specimens were placed back in a 6-inch by 12-inch cylinder mold, and the other half of the cylinder was cast with grout. The method of mixing the two types of grouts is explained in the grouting processes. Specimens were ponded with water prior to grout casting. Water was removed immediately before grout placement, and the concrete surface dried to be free of standing water. All the cylindrical specimens were cured in a moist fog room following demolding 48 hours after casting.

Specimens were prepared by slicing the 6-inch by 12-inch cylinders down to a 6-inch by 3-inch slice to expose the surfaces of the concrete and grout material to salt water. A first coat of epoxy paint was applied to all the specimens along the cylindrical face and bottom. After 24 hours, a second coat of epoxy paint was applied perpendicular to the first coat's direction. The dried painted specimens were exposed to a lime water bath for 48 hours before saturating with salt water (salt curing) per ASTM C1556.

3.2.5.2 Saltwater Exposure

According to ASTM C1556, a 165-gram/liter salt solution was prepared using deionized water and technical-grade sodium chloride. A large container was used to accommodate all the test specimens. All specimens were submerged in the salt solution for 35 days. Samples were removed from the salt solution and cured in the ambient air until profile grinding at a laboratory temperature of 68 ºF.

3.2.5.3 Chloride Profiling

Profile grinding was conducted using a milling machine with a 5/16-inch diameter concrete coring bit to obtain powdered samples (Figure 18). Eight-layer thicknesses were ground in 1-millimeter increments in each constitutive material and along the concrete-grout interface for each surface

preparation technique. Two specimens were used for the constitutive material and four specimens for the concrete-grout interface to obtain a ten grams powder. Samples not exposed to saltwater were milled to determine the initial chloride concentration. The profile milling was performed to gather sample material for chloride profiling, conduct acid dissolution, determine equivalence point, and obtain chloride content at several depths by titration with silver nitrate using an auto titrator per ASTM C1152 (Figure 16). A nonlinear regression analysis was performed on the data to determine the diffusion coefficient.

(a)

(b)

(c)

Figure 18. Ion Permeability Testing: (a) Samples after exposure to salt water, (b) determining acid soluble chloride content, and (c) milling samples

3.2.6 Ultrasonic Pulse Velocity Test (UPV)

Ultrasonic pulse velocity test was performed on 6 in. x 6 in. x 10.5 in. prisms and 4 in. x 8 in. cylinders. Both types of specimens were half concrete and half grout. The UPV test was conducted to determine the transit time in µsec closer to the interface and away from the interface with an interval of 2 inches. Direct and indirect UPV transmission methods were employed (Figure 19). The test was performed in accordance with ASTM C597 standard (ASTM C597) (Figure 3). The semi-direct transmission method was conducted on the prism specimens, and the direct transmission on the cylindrical specimens.

(a) *(b)*

Figure 19. UPV Testing methods (a) Direct method on prisms(b) Indirect method on cylinders

3.2.7 Microstructural Analysis

The microstructural analysis utilizes scanning electron imagery to quantify the porosity at the interface. Porosity at the interface and the constituent materials significantly influences the strength and other properties. A high porosity at the interface is detrimental to the strength and permeability, mainly if the voids are large and connected. Therefore, the porosity value at the interface provides valuable information, particularly on the durability characteristics.

3.2.7.1 Specimen preparation

Grout-concrete specimens were cored and prepared for microstructural analysis. The cores of 2-inch diameter were extracted with the interface exposed. Six (6) samples were extracted to perform this test. Specimens were dried to remove any remaining water particles is necessary since the water particles can interfere with the polymerization of the stabilizing epoxy (described below). The samples were immersed in isopropanol for 48 hours after coring and dried in an oven at 50 ºC (Figure 20).

Figure 20. Extracted 2-inch diameter samples drying in oven

Epoxy Impregnation

Before performing polishing and grading, it is essential to keep the pore structure and stabilize the microstructure with epoxy (Stutzman & Clifton, 1999). The specimens were vacuum-impregnated by placing them in a container and surrounded with a general purpose MAX 1618 A/B low viscosity (LV) epoxy resin. The LV epoxy resin comes in two compound parts, part A and part B. the part A is a thinner, less viscous resin and part B, the hardener. Properties of the epoxy resin is presented in appendix B. Prior to the impregnation stage, the specimens were stored in a vacuum oven to stop hydration within the samples. Air entrapped in the epoxy were removed by placing it in a vacuum chamber and removed by a water jet pump preceding to the impregnation. The specimen was placed in the vacuum chamber and the epoxy resin is pumped. The sample is covered with epoxy and pushed further into the pore system of the specimens (Figure 21). The samples were cured for at least 24-hours after the epoxy impregnation.

Figure 21. Epoxy impregnation

Grinding, Lapping, and Polishing

The epoxy impregnation is followed by careful grinding, lapping, and polishing (Figure 22). This step is carefully done since it can significantly affect the images and results of the microstructural analysis. A succession of grinding and polishing steps of progressively finer abrasives was performed to obtain a flat-polished surfaced specimen for imaging. Smoother surfaces are gradually obtained at each grinding and polishing stage, with the deformation produced by previous grinding and polishing stages sequentially removed.

The first stage of the grinding method was to remove excess epoxy. This was done with a 70-µm dia-grid diamond disc. The final stage of the grinding involved grinding on a 30- µm and a 15-µm dia-grid diamond disc. Lapping was performed with 9-µm and 6-µm diamond grit suspensions. Extreme care was taken during the grinding and lapping. Polishing was performed with three grades of diamond polishing grit suspensions (3-µm and 1-µm). Final polishing was performed with two 0.005-µm diamond grit polishing suspensions, colloidal alumina and silica.

Figure 22. Grinding, lapping, and polishing of samples

It was essential to examine the specimens in an optical microscope in a reflected light mode to assess the effect of the preparation stages (Figure 23).

Figure 23. Assessing specimen after grinding, lapping, and polishing stages

The polished specimens were kept in an oven vacuum to fully dry prior to imaging.

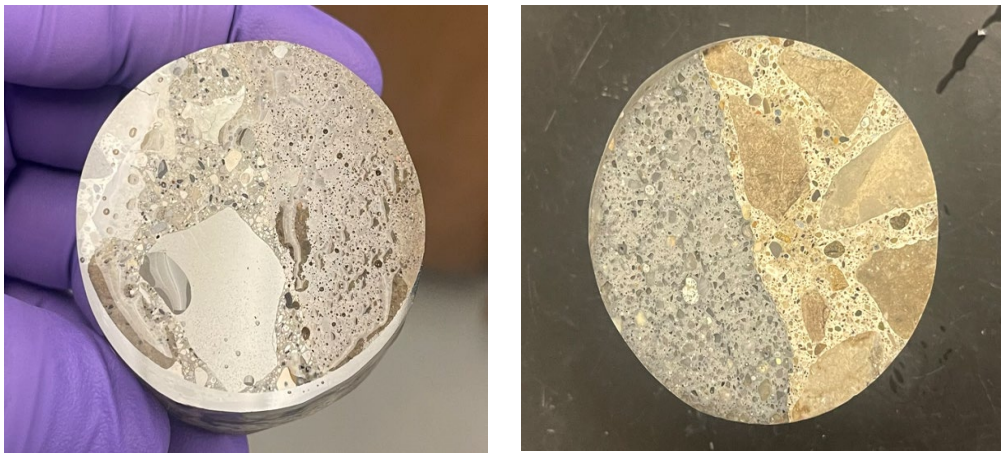

(a) *(b)*

Figure 24. Polished samples

3.2.7.2 Imaging

After preparing the sample, the microstructure of the polished specimens was examined using Quattro S scanning electron microscopy (SEM). Images were collected using the backscattered electron detector. The process was performed under a low vacuum detector (LVD) because the specimens were non-conductive at 20 kV and a 10-mm working distance. Each map had an area of 24 tiles, stitched together to make a large BSE map with a total area of 216 fields. Each tile set has an area of 3.54 mm^2. Large backscattered electron (BSE) areas were collected using Maps 3.11 microanalysis software. For each specimen, nine (9) maps were taken. An image analysis methodology detailed by Beyene et al. (2017) was adopted for the treatment process of the images. An example of the large BSE map for the constitutive materials is presented in (Figure 25).

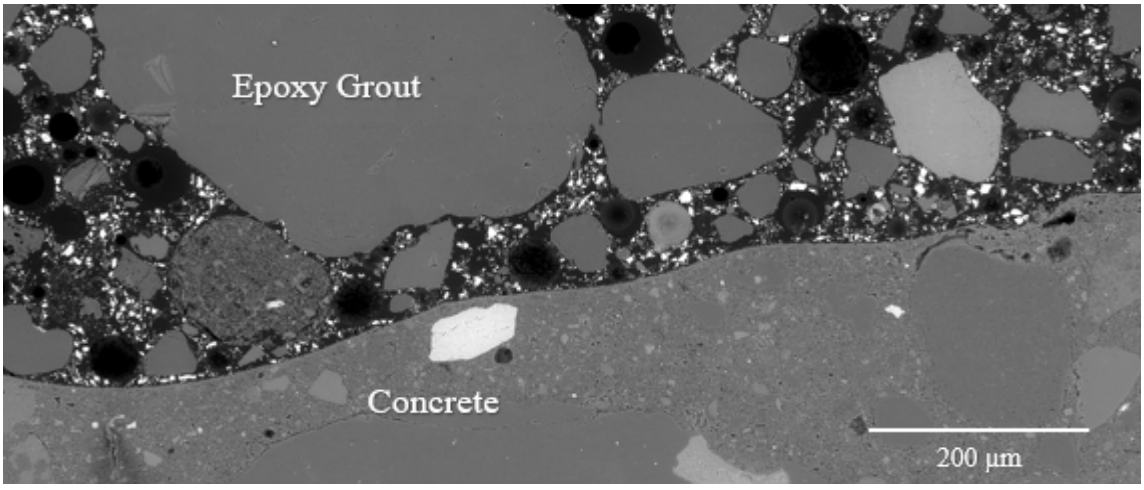

(a)

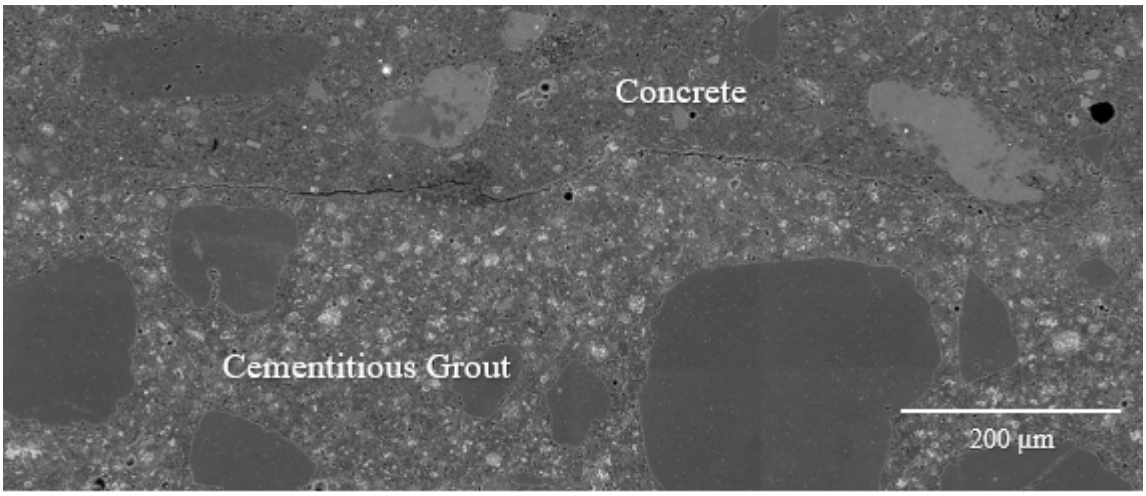

(b)

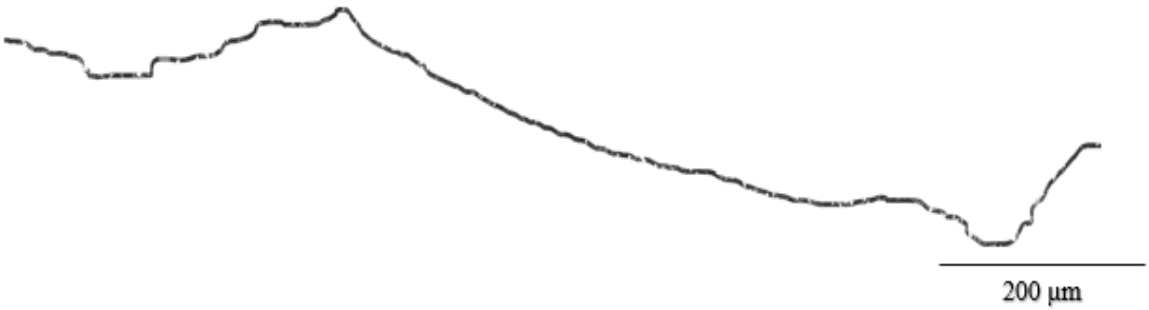

(c)

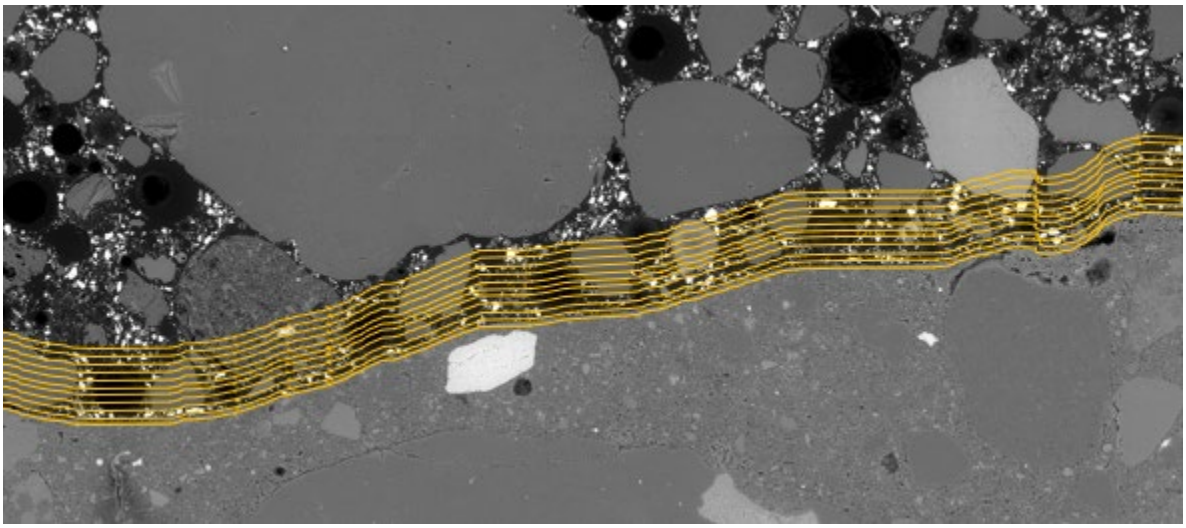

(d)

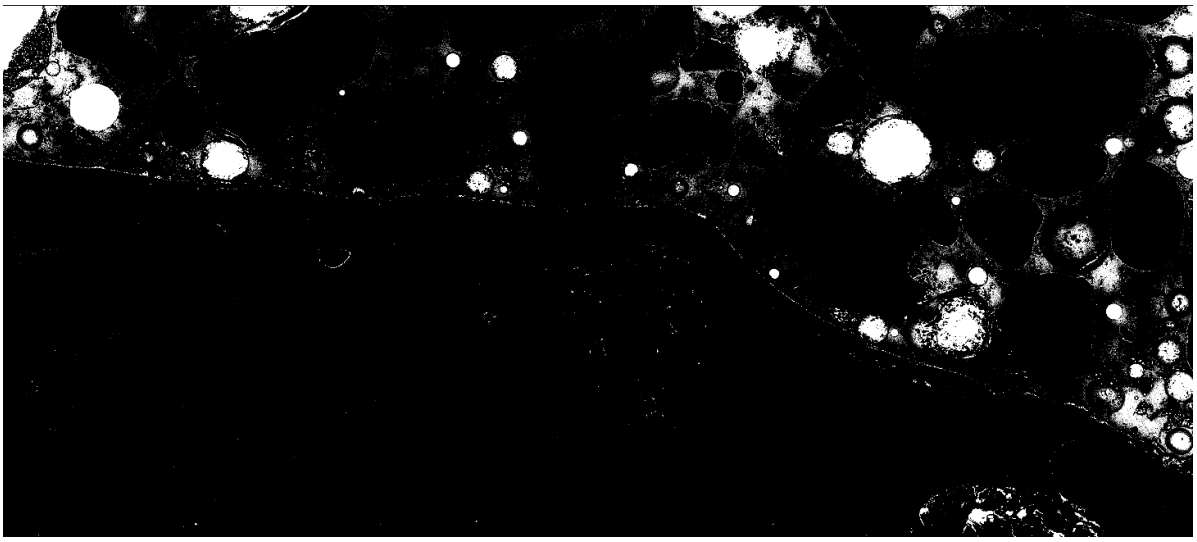

(e)

Figure 25. (a) and (b) Large BSE map, (c) Location along interface of 10-µm wide bands,(d) A 10-µm wide band extracted from exposed aggregate surface example, and (e) Example of the segmentation process

A porosity profile was obtained on the images by extracting successive 10-µm wide bands (Elsharief et al., 2003) in the grout. Segmentation was performed on the obtained original large BSE map for porosity measurements. The porosity measurements were evaluated on the constitutive grout material (epoxy and cementitious grout) adjacent to the surface of the substrate up to 100-µm and a 10-µm in the substrate to determine the porosity measurement based on the type of surface preparation. An example of a segmentation process and a typical 10-µm wide bands are presented in Figure 25(d) and (e), respectively. An image analysis software Mipar was used to quantify the porosity in each of the BSE 10-µm wide bands. The same process detailed by Beyene et al. (2017) was used to measure the porosity.

RESEARCH FINDINGS AND CONCLUSIONS

Results

4.1 Chloride Profiling

Chloride profiling was conducted as per ASTM C1556, with chloride contents at each point determined by ASTM C1152. Profiles were measured after 35 days of saltwater exposure for the three constitutive materials and each interface experimental group (concrete, cementitious, and epoxy grout). Least squares regression was then utilized to determine the material's apparent diffusion, Da, and to predict the concentration of chloride ions at the surface of test samples. Figure 26 presents an example of the measured chloride profile and non-linear regression analysis for epoxy grout interface specimens with no surface preparation. Results for each experimental group are presented in Table 4. The data points represent the minimum average of each sample at an average depth from the exposed surfaces. Each of the material's initial chloride content, C_i, before the exposure to salt water, is presented in the table; the C_s is the estimated chloride content of the material at its exposed face. Figure 27 presents the apparent diffusion coefficient, and Da for each constitutive material and interface region.

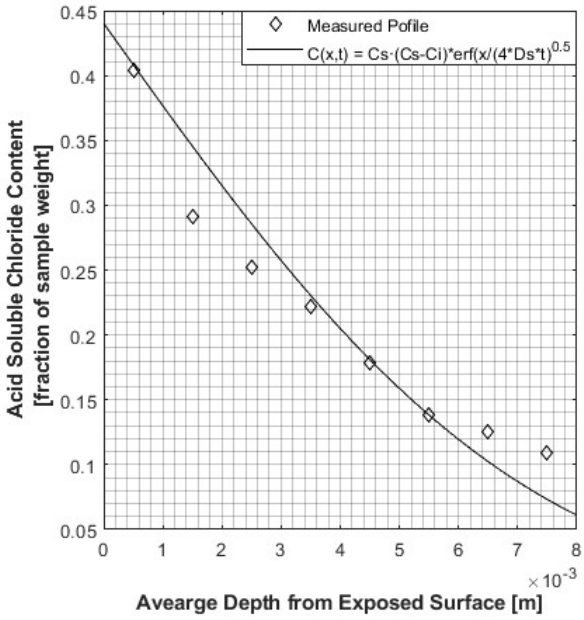

Figure 26. Epoxy Grout with no surface preparation chloride - sample diffusion Profile

Table 4. Chloride Profiling Results

Material		Initial Chloride Content, Ci [% sample weight]	Calculated Surface Chloride Content, Cs [% Sample Weight]	Apparent Diffusion Coefficient, Da [m^2/s]
Concrete		0.0442	0.7308	5.412E-12
Epoxy Grout		0.0030	0.4401	3.280E-14
Cementitious Grout		0.0306	0.7219	1.397E-12
Interface Specimens	Sand-blasted Epoxy Grout	0.0457	0.4483	4.073E-12
	Epoxy Grout with no preparation	0.0439	0.4401	5.156E-12
	Water-blasted Epoxy Grout	0.0447	0.4401	5.341E-12
	Sand-blasted Cementitious Grout	0.0365	1.6794	1.957E-12
	Cementitious Grout with no preparation	0.0420	0.6522	5.544E-12
	Water-blasted Cementitious Grout	0.0386	0.5202	4.118E-12

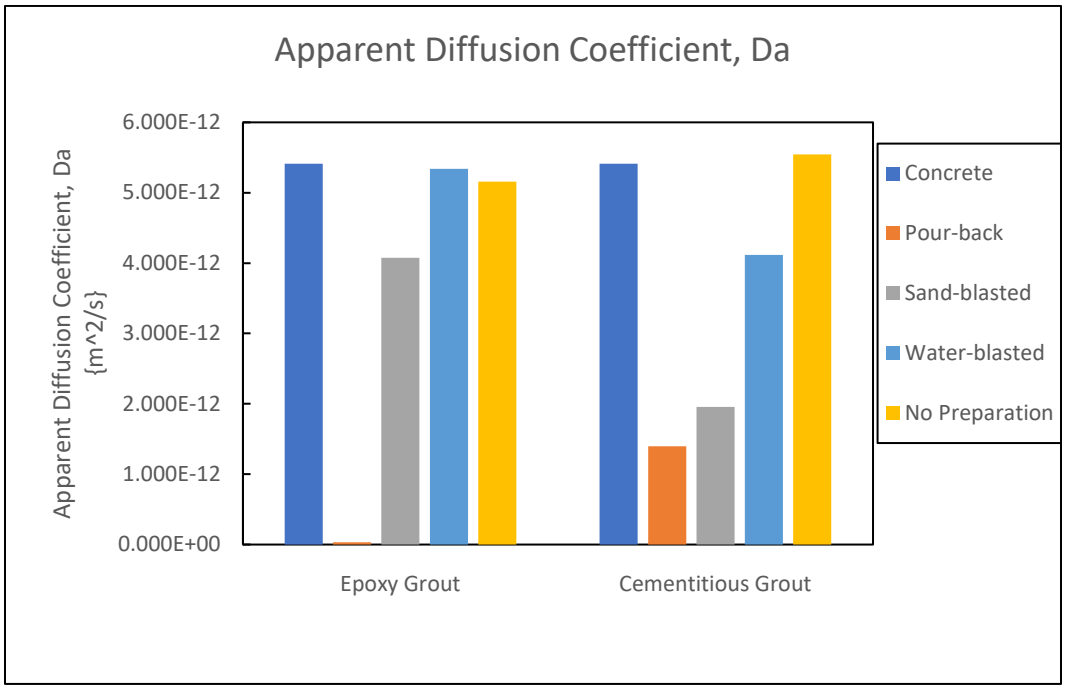

Figure 27. Apparent Diffusion Coefficients

The diffusion coefficient measures how rapidly ions can diffuse through a material. A lower diffusion coefficient indicates that ions will take longer to diffuse through the material and is correlated to greater durability of the material.

Initial chloride concentrations, C_i ranged from 0.0030% by sample weight (epoxy grout) to 0.0457% by sample weight (concrete-cementitious grout sandblasted interface specimen). For the concrete mix design utilized, there was an initial chloride content of 0.19% by weight of cement; this is greater than the recommended limit prescribed by ACI 222 for prestressed concrete construction (0.08%), but less than that prescribed for ordinary reinforced concrete in severe exposure (0.20%) (ACI-222.2R-01). It is important to note that while the measured initial chloride content of the concrete was outside of recommendations for post-tensioned concrete, this study sought to characterize chloride ion diffusion, which is mimimally impacted by the increased chloride ion presence as the diffusion model considered by ASTM C1556 does not generally consider chloride ion binding.

The calculated surface chloride contents, C_s, range from 0.4401 to 1.6794% by sample weight and are in agreement with values reported by Song et al. and Burris & Riding (Burris & Riding, 2014; Song et al., 2008). High surface ion contents are expected because this is the exposure face. The epoxy grout and the epoxy interface specimens recorded the lowest Ci (0.4401% - 0.4483%), indicating a low likelihood of chloride concentration throughout the sample.

The calculated diffusion coefficient for concrete was 5.4E-12 m^2/s. The diffusion coefficients for the grout were 3.3E-14 m^2/s and 1.4E-12 m^2/s for epoxy and cementitious grout, respectively. The diffusion coefficients of all the interface specimen experimental groups but for cementitious grout, no preparation were determined to be between concrete and grout. These results were anticipated as the chloride profiling technique for the interface region required milling approximately 2 mm of material on either side of the interface (grout and concrete). Epoxy grout water blasted, and no preparation interface experimental groups had diffusion coefficients very close to concrete, whereas sand blasted was reduced. Cementitious grout, however, both the sand and water blasting techniques had diffusion coefficients less than those of epoxy grout counterparts, possibly due to the increasing matrix of cement hydration products along the interface during curing. However, cementitious grout with no preparation had a diffusion coefficient higher than that of either constitutive material. This suggests that this interface is more susceptible to chloride ion intrusion than either of the constitutive materials and could serve as a "fast track" for chloride ions to initiate corrosion of the PT anchorage. This is probably due to localized increased porosity at the interface and a lack of mechanical interlock between materials. It is desirable for the material interface between concrete and grout to have a predicted diffusion coefficient that is less than that of concrete to mitigate the risks of premature corrosion of the anchorage.

4.1.1 Time required to initiate corrosion

In order to illustrate how the apparent diffusion coefficients correspond to the durability of a concrete structure, the time required to initiate corrosion of a mild steel reinforcement was modeled with Life-365 service life prediction model software. This concrete life cycle assessment model was developed by a consortium including the American Concrete Institute (ACI) and was released

in August 2001. The apparent diffusion coefficient for each constitutive material and the sample interfaces was input, considering a 12-inch square column and a 2-inches of clear concrete cover. The chloride exposure modeled was based on an urban highway bridge in Columbus, Ohio.

Concrete recorded the lowest predicted time required for corrosion initiation of 38 years for the constitutive materials, followed by the cementitious grout at 127 years. The epoxy grout was estimated to have the greatest time to corrosion initiation (156 years, Figure 28).

For the concrete-epoxy grout sample interfaces, the sand-blasted surface preparation was estimated to have the greatest time to corrosion initation at 70 years. No surface preparation was predicted to resist corrosion for 55 years, and the water-blasted surface preparation at 54 years (Figure 28. The concrete-cementitious grout sample interfaces showed the sand blasted surface preparation of 78 years, water blasted surface preparation, 41 years and the no surface preparation showed 32 years required for corrosion initiation (Figure 28).

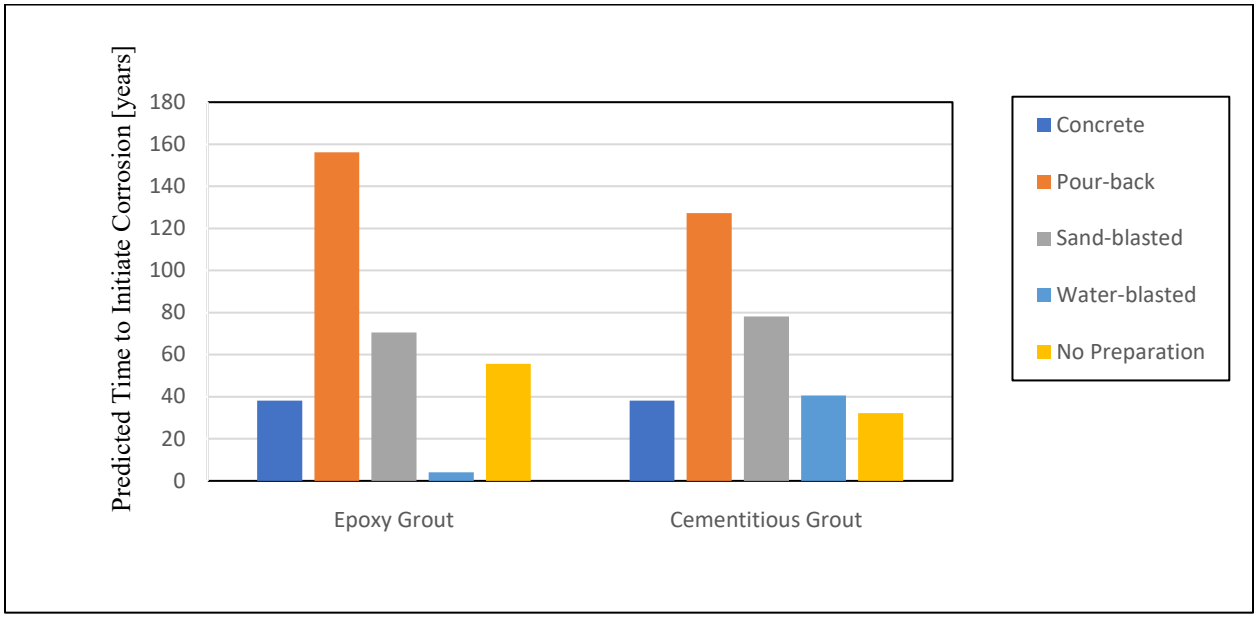

Figure 28. Predicted time to initiate corrosion

4.2 Pull-Off Testing

Pull-off testing was performed on the slab specimens when the substrate (concrete) was 90 days old and the grouts (epoxy and cementitious) were 60 days old. Figure 29 presents results from 90-day pull-off testing. All failure modes observed were interface failures. Epoxy grout pull-off strengths were measured to be greater than cementitious grout strengths; many test samples within the no-preparation and water-blasted groups did not fail at 580.2 psi, the capacity of the test equipment. Epoxy grout sand blasted interfaces failed at an average strength of 261.1 psi. Three additional test sites experienced glue failure during the pull-off testing, and these results are not presented in the results. Because these failed at higher stress than the average interface failure, it is expected that the interface is stronger than 261.1 psi. It is possible that moisture during surface preparation did not penetrate the surface of the concrete substrate in the no-preparation epoxy grout

group. Because epoxy is water insoluble, it is possible that this produced better epoxy penetration in the no-preparation and water-blasted test specimens and higher tensile strength.

Cementitious grout pull-off strengths were significantly lower. In fact, during coring on the concrete-cementitious grout, five of seven cores attempted in the no surface preparation broke off during the coring, indicating insufficient strength for testing. The average strength of the two remaining cores was 43.6 psi. Sand-blasted cementitious grout specimens exhibited a strength of 57.7 psi, and water-blasted specimens exhibited an average pull-off strength of 150.4 psi. All the pull-off strengths of the concrete-cementitious grout interface specimens were lower than the minimum pull-off value specified by ODOT of 175 psi (State of Ohio Department of Transportation, 2014).

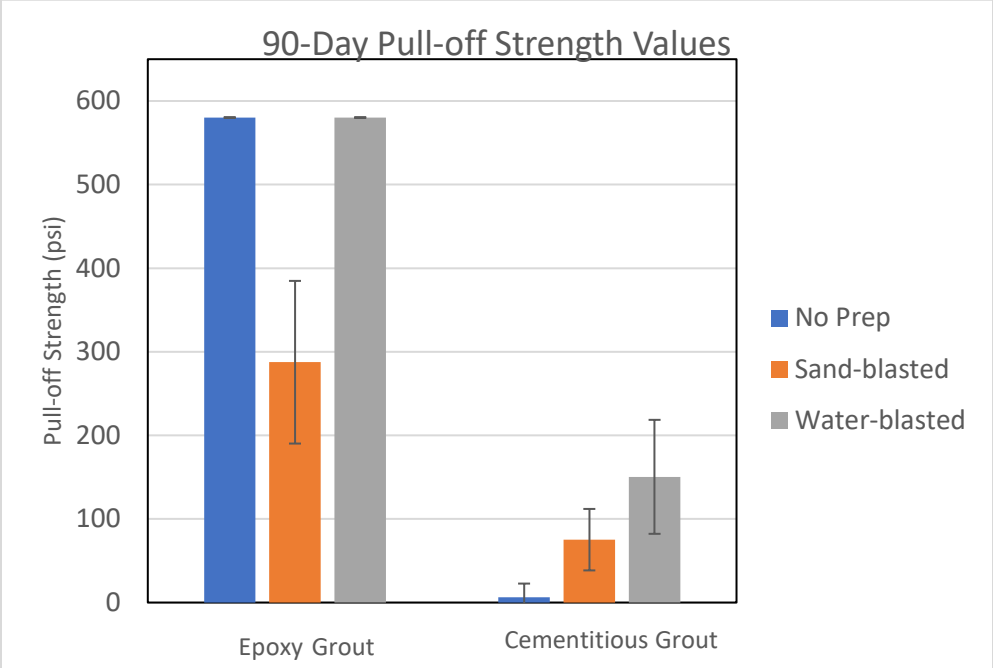

Figure 29. Pull-off Test Results

4.3 Ultrasonic Pulse Velocity (UPV)

Ultrasonic pulse velocity (UPV) was conducted to determine if interface adhesion defects could be detected by this easily implemented field test. Testing was conducted at various lengths from the interface to determine if the distance from the interface influenced the UPV results. The results of the UPV test conducted in general agreement with ASTM C597 (specimen geometry was different) are presented in Table 5 prism specimens and Table 6 for cylindrical specimens. UPV of prism specimens was conducted via the "indirect" method, while cylindrical specimens utilized the "direct" method (Figure 30). While prism specimens were cast for each experimental group,

cementitious grout samples in the no-preparation and water-blasted groups fractured during testing, so results for these prisms are not presented.

Table 5. UPV results for prism specimens

Material		Average UPV transit time (µsec)	Average UPV (in/µs)
Prism Interface Specimens	Sand-blasted epoxy grout	74.94	0.139
	Epoxy grout with no preparation	69.41	0.11
	Water-blasted epoxy grout	97.06	0.4401
	Sand-blasted cementitious grout	57.01	0.178

Table 6. UPV results for cylindrical specimens

Material		Average UPV transit time (µsec)	Average UPV (in/µs)
Cylindrical Interface Specimens	Sand-blasted epoxy grout	30.06	0.15
	Epoxy grout with no preparation	31.55	0.144
	Water-blasted epoxy grout	28.13	0.186
	Sand-blasted cementitious grout	25.22	0.175
	Cementitious grout with no preparation	25.69	0.175
	Water-blasted cementitious grout	25.07	0.179

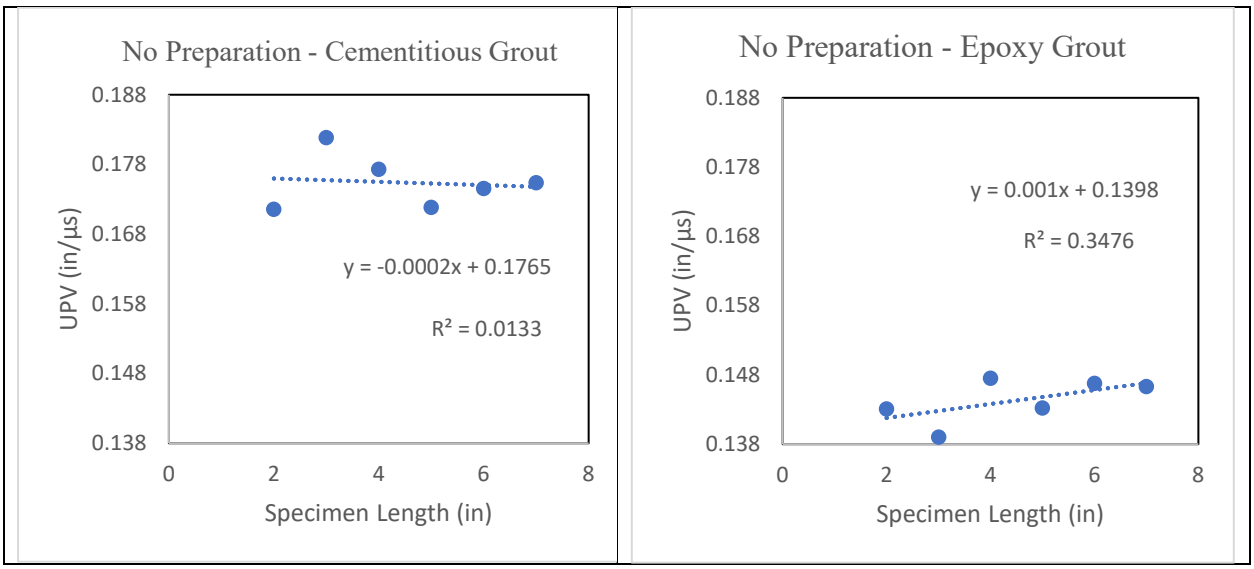

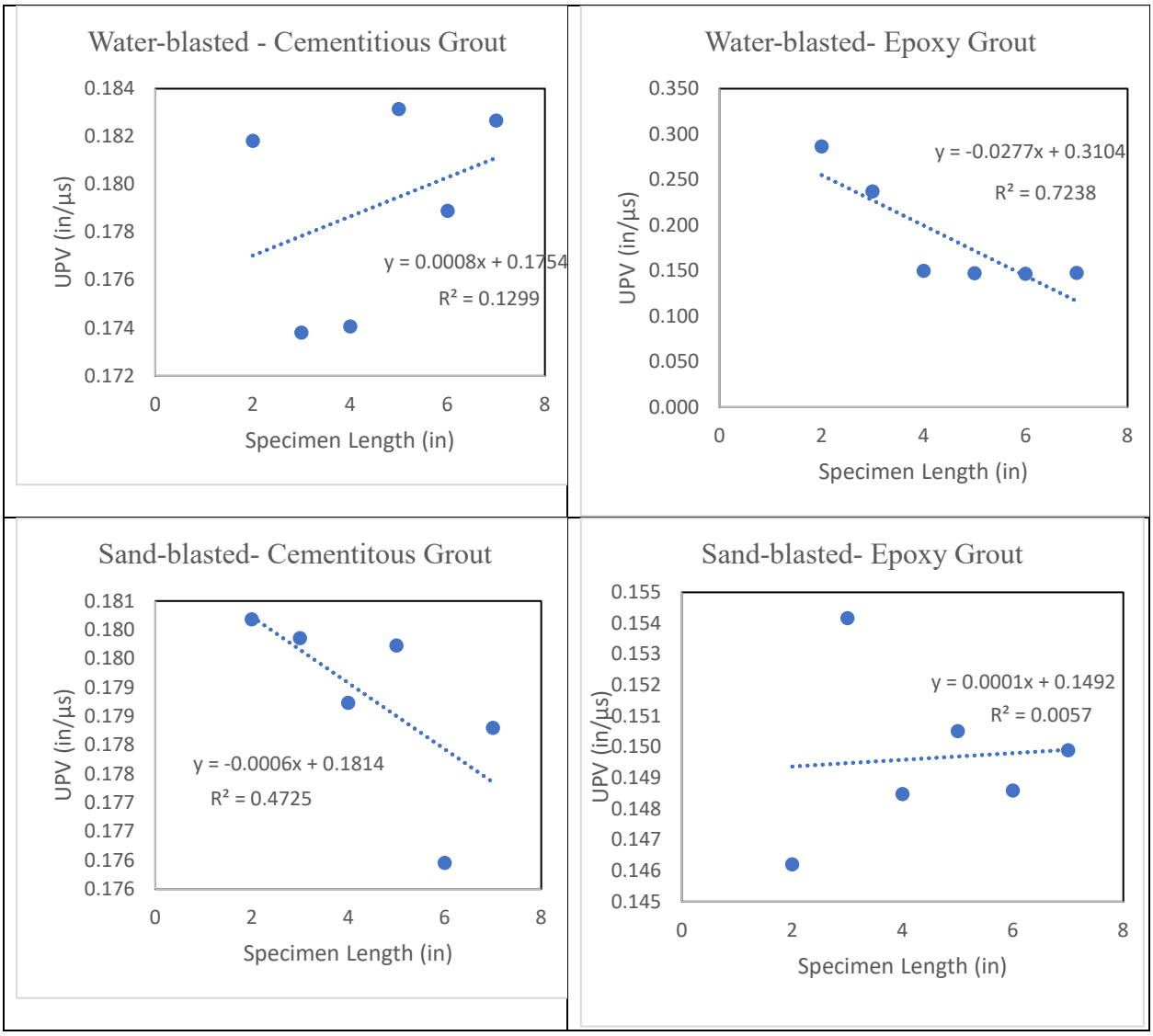

Figure 30. UPV transition times in test specimens

UPV values ranged from 0.11 to 0.44 in/µs. With two exceptions (water blast cementitious grout and no preparation epoxy grout), the UPV generally decreased with increasing distance to the interface. However, r-squared values were relatively low, indicating high variability within the test. Smaller changes were observed with increasing length in prism specimens than cylindrical specimens, as evidenced by smaller slopes in the regression lines. Based on the experimental laboratory tests, and the high variability in the results, UPV is not sensitive to the interface preparation techniques and the grout type.

4.4 Microstructural Analysis

The microstructural analysis of the grout-concrete interface was performed on 2-inch diameter cored samples extracted from 90-days old concrete and 60-days old grouts of 6" diameter cylinder specimens. Both the concrete substrate and grout material were evaluated. The interface between the substrate and the grout was seen as a line bisecting the test specimen during the imaging. For

this work, the interface region was considered an area, evaluated in 10-um wide bands extending from the interface. The grout material was evaluated at a distance extending 100 μm from the interface, and the concrete was evaluated only within the first 10 μm from the interface, similar to (De La Varga et al., 2018).

The total porosity distribution of the grout is measured as a function of the distance from the concrete surface (Figure 31). The results include two constitutive materials (cementitious and epoxy grout) and three surface preparation methods at the interface (water jetting, sand blasting, and no surface preparation).

In concrete-cementitious grout samples, porosity linearly decreased with increasing distance from the material interface. Concrete-cementitious grout samples with no surface preparation (CG-N) showed significant porosity values within the analyzed 100 μm band. A value of 21% was measured as the porosity in the first 10 μm (0 μm to 10 μm) wide band from the concrete surface. At 20 μm (10 μm to 20 μm), the measure porosity value was 20%. The porosity values gradually decreased moving away from the concrete interface to a value ranging from 10% to 12% at 100 μm from the interface. The higher porosity measurements determined in the 10 μm to 20 μm band in the CG-N specimen are likely caused by higher capillary pores. The other concrete-cementitious grout samples with water-blasted (CG-W) and wet sand-blasted interfaces (CG-S) showed a similar trend as the CG-N but with a lower magnitude. All the measured porosity values within 100 μm on the CG-N were greater than those measured in any other experimental group. The CG-S porosity values ranged from 5% to 2.7% for the first 20 μm wide bands, reducing to 1.6% at 100 μm from the interface. CG-S values ranged from 6% to 3.5% in the first 20 μm wide bands. This also reduced to 3.2% at 100 μm from the interface.

Porosity measurements for epoxy grout specimens at the interface were generally significantly less than those of cementitious grout specimens of the same surface preparation. Porosity exhibited a non-linear trend with increasing distance from the interface for all epoxy grout specimens; porosity generally increased linearly until 60 μm from the interface and then decreased linearly. Porosity measured within the first 10 μm band from the interface were greatest for EG-N at 6% compared with 2.9% for EG-S and 0.1% for EG-W. However, EG-S and EG-N specimens' porosity values decreased at 20 μm. The EG-S did not decrease at the 20 μm band.

Porosity measurements were also taken in the concrete substrate within the first 10 μm from the interface (Figure 32). The concrete with no surface preparation exhibited a high porosity value (17.4%). This value decreased significantly to 1.9% for the sandblasting surface preparation, and the water jetting recorded a value of 0.8%.

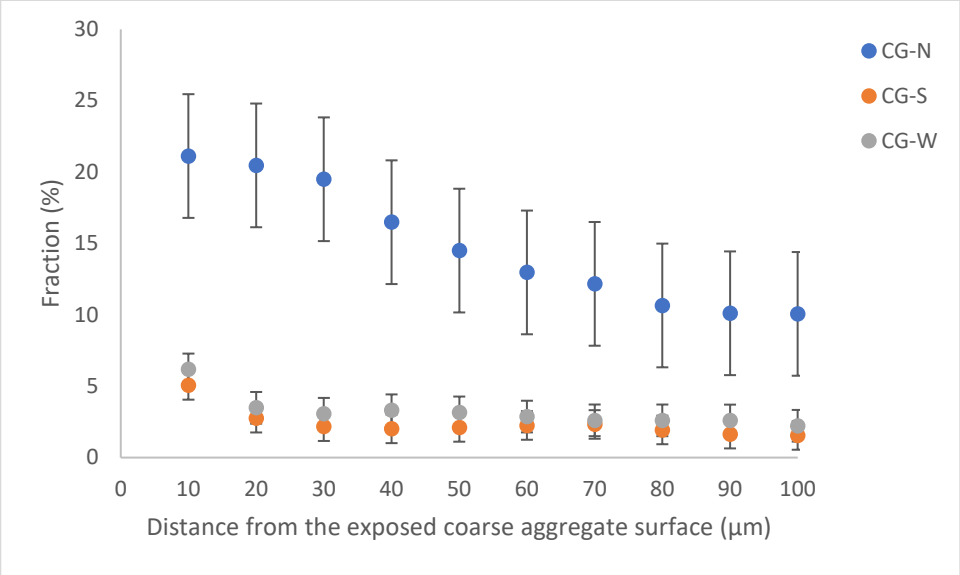

(a)

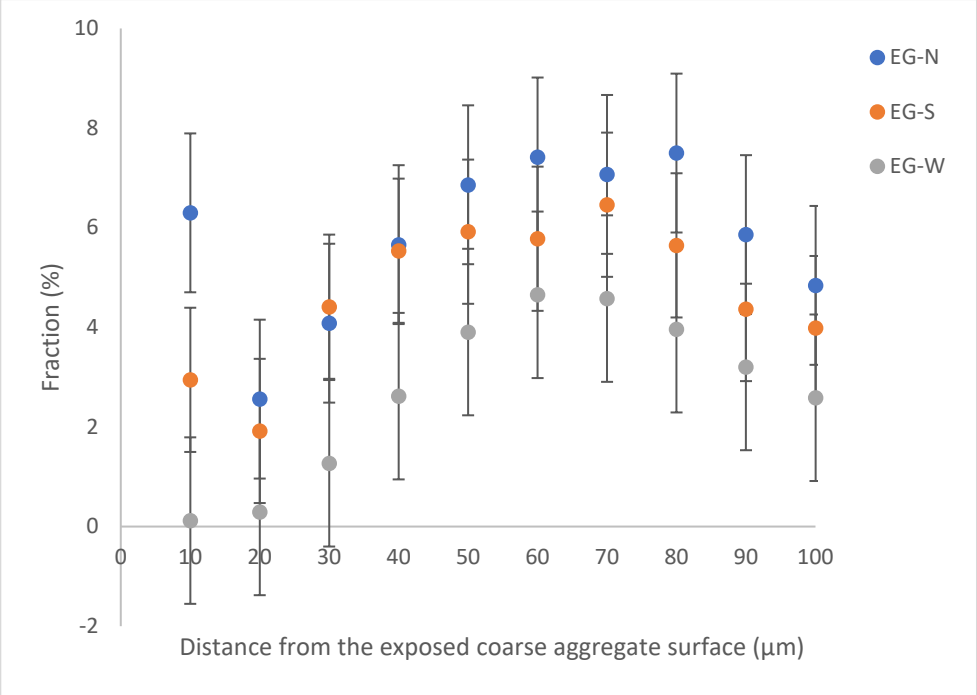

(b)

Figure 31. Overall porosity distribution in (a) Cementitious grout and (b) Epoxy grout

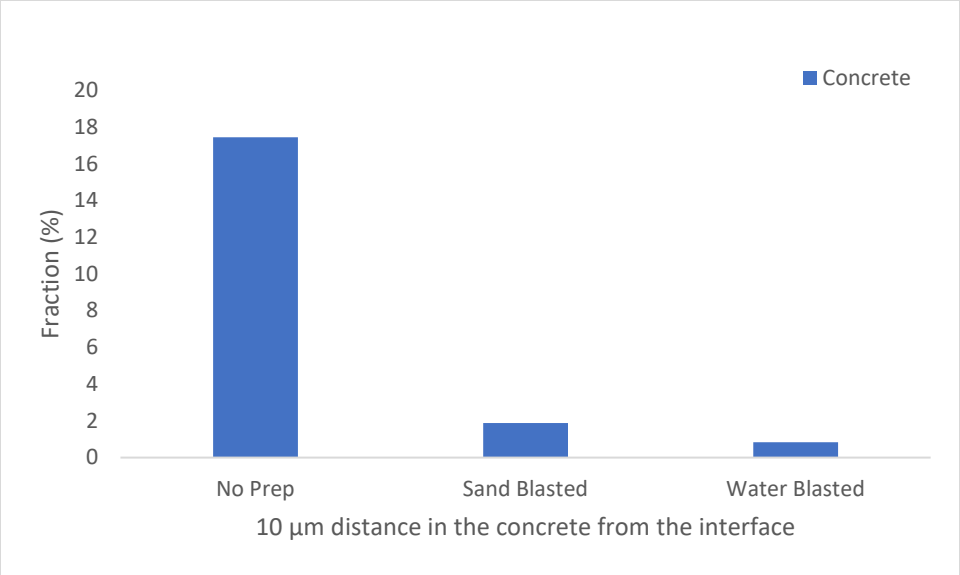

Figure 32. Porosity measurement at 10 µm of the concrete

DISCUSSION

For the determinations of specifications and testing approval, understanding the relationship between bond strength and chloride permeability, bond strength and porosity, and porosity and UPV are necessary.

1.1 Bond Strength vs Chloride Permeability

The surface preparation method likely has a substantial influence on the both the interfacial mechanical strength and the chloride ion permeability. The investigated surface preparation methods show significant differences in the bond strength and to an extent, the chloride ion permeability. For performing this investigation, the results of the 90-day pull-off test were plotted against the apparent diffusion coefficients calculated from the chloride profiling for the interface specimens (Figure 36). The plot also included the constitutive material and the average between them.

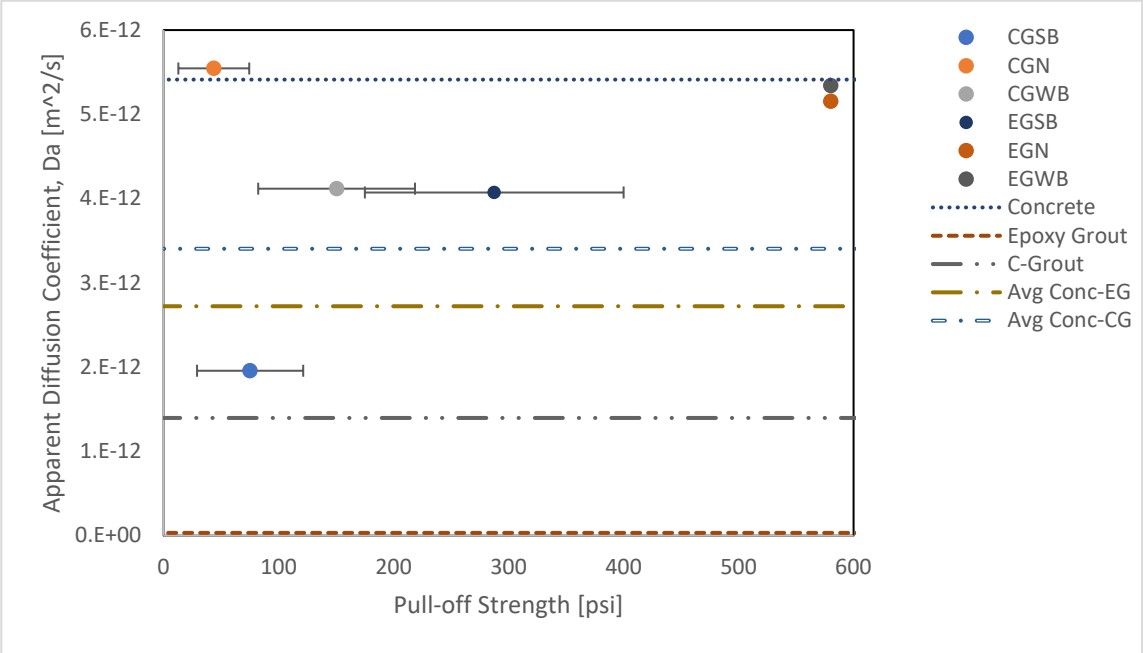

Figure 33. Apparent Diffusion Coefficient vs Pull-off Strength

A higher apparent diffusion coefficient represents a higher chloride ion permeability as the material provides less resistance to ion intrusion. Generally, a well-performing interface should meet minimum strength and have a lower apparent diffusion coefficient than concrete. Some specifications set the minimum strength at 175-psi (State of Ohio Department of Transportation, 2014). Though guidance is not provided as to the justification for this strength, this likely provides sufficient mechanical interlock. Diffusion coeffcients below that of concrete indicate that the expected chloride ion intrusion along the interface would not exceed that of concrete and that the interface is not a “fast-track” for ion intrusion. Three experimental groups meet both of these criteria: EGSB, EGN, and EGWB. None of the cementitious grout interfaces met the minimum strength requirements, and the diffusion coefficient of CGN exceeded that of concrete. In both

grout materials, the sand blasted group had a lower diffusion coefficient than other experimental groups but less than the maximum pull-off strength for that material. While not formally correlated, high pull-off strength does relate to greater resistance to chloride ion intrusion.

1.2 Porosity vs Pull-off Strength

Bond interface is generally considered as the weakest link due to high porosity and microcracks (Elsharief et al., 2003). Defects located at concrete interfaces, such as pores and micro-cracks result in less effective bonding of secondary pour materials. Surface preparation of a concrete interface is assumed to influence the porosity of the interface (De La Varga et al., 2018). The bond strength of the interface specimens exhibited different values. In most cases, the abrasive surface preparation technique had greater pull-off strengths than no surface preparation, or waterblasted preparation. SEM images and porosity profiles of the grout along the interface specimens were considered to better comprehend the mechanism behind the improved bond strengths for some of the specimens. In examining this idea, 90-day-pull off test were plotted against the average porosity values at 100-µm and 10-µm calculated from the microstructural analysis presented in figure 34 and 35 .

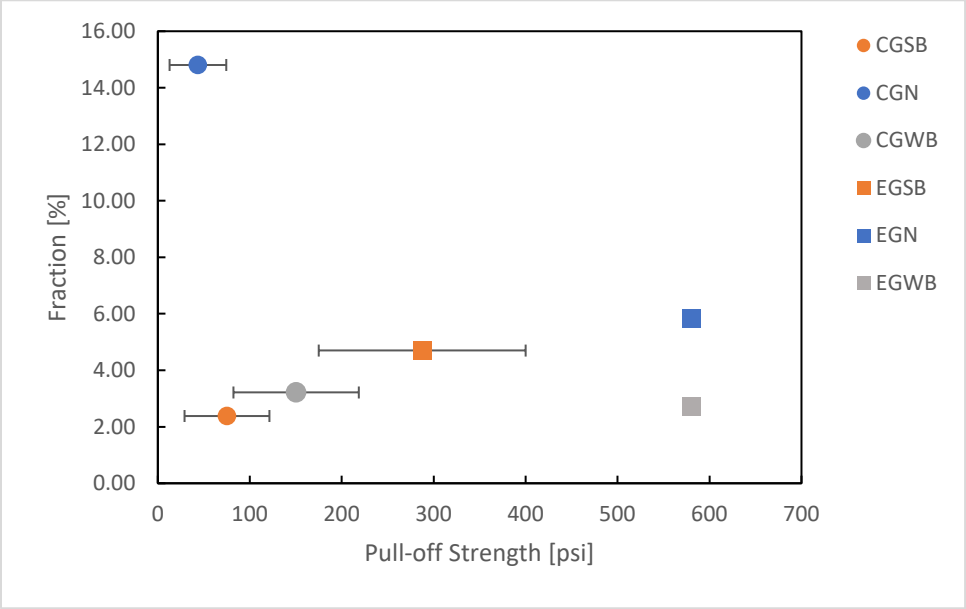

Figure 34. Porosity a t 100-µm vs Pull-of Strength

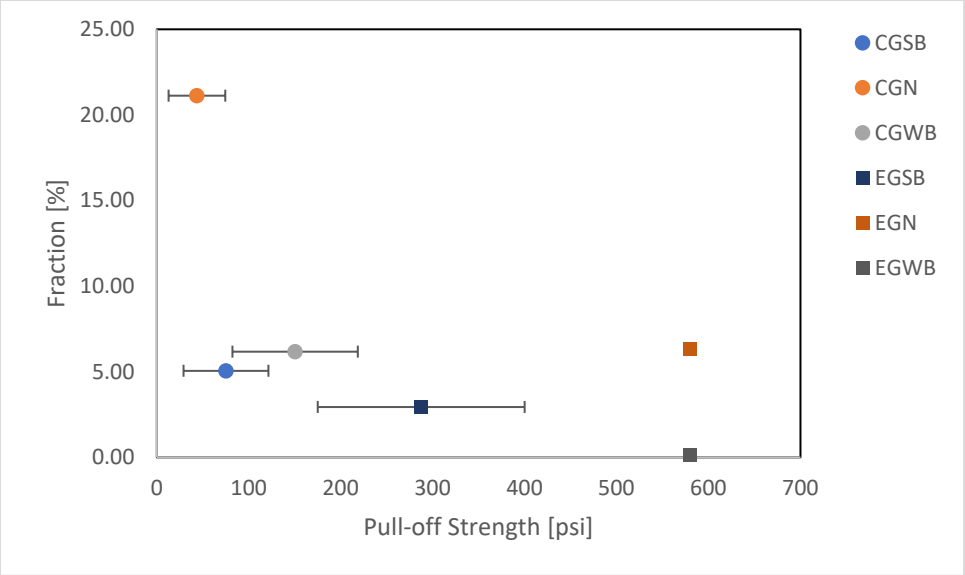

Figure 35. Porosity at 10-µm vs Pull-of Strength

Cementitious grout employs cement hydration reaction in forming hydration products that interact with the surface of the concrete substrate (Tatum et al., 2021). The surface preparation techniques provided an exposed coarse aggregate, and as such, two different types of surfaces were present for the concrete-grout contact, i.e. coarse aggregate and concrete paste surfaces (De La Varga et al., 2018). The SEM images of the cementitious grout interface specimens displayed particle packing deficiencies, which may be credited to non-optimum gradation of sand and fillers during the grouting (De La Varga et al., 2018), though other causes may exist. Surface preparation techniques appeared to aid in addressing these deficiencies. While the no surface preparation interface specimen exhibited significant average porosity value, the sand and water-blasted specimens had significantly lower porosity values. The no surface preparation interface specimen exhibited low bond strength, whiles the sand and water-blasted interface specimen exhibited greater bond strength values, though less than the specified minimum as stated earlier. This goes in agreement that providing a great abrasive surface preparation technique is valuable to the interface area, which can improve the porosity properties and bond performance – if only assessed from a mechanical test such as pull-off testing. In addition, the water moving from the grout into the concrete may have reduced the grout's hydration through the reduction of available water needed for the reaction. In this case, the interface may become a plane for mechanical weakness (Tatum et al., 2021).

Alternatively, in the epoxy grout interface specimens showed low porosity values, the water-blasted had the least porosity and the no surface preparation interface specimen had the greatest porosity. In this situation, the surface preparation is relevant to the bond mechanism. With the epoxy grout specimens, epoxy serves as low viscosity glue which suffuses the concrete surface and fills voids. The SEM images of the epoxy grout specimens hardly showed defects such as micro-cracks. The bond strength for the epoxy grout interface specimens showed average significant values of 580.2-psi for both the EGN and EGWB, and 287.5-psi for the EGSB, which were greater than the specified minimum. The presented data shows that the greater bond strength

may or may not correlate low porosity values. This makes sense because as stated earlier, when pores are interconnected with a high porosity, permeability is high, but if pores are disconnected, permeability is low, though, porosity is high (Kearsley & Wainwright, 2001).

1.3 Ultrasonic Pulse Velocity (UPV) vs Porosity

Little previous work has evaluated on the relationship between UPV and porosity. Lafhaj et al. (2006) presented a correlation between UPV and porosity for mortar (Lafhaj et al., 2006), and found to be an inverse correlation between these parameters. . A reduction in UPV may indicate that there are pores in the concrete structure (Yaman et al., 2002), indictaing an inverse proportionality between UPV and porosity . It is expected that UPV values decrease with increasing porosity. The average porosity at 100-µm, and 10-µm verses the average UPV results for cylindrical specimens are shown for each experimental group in figure 37 .

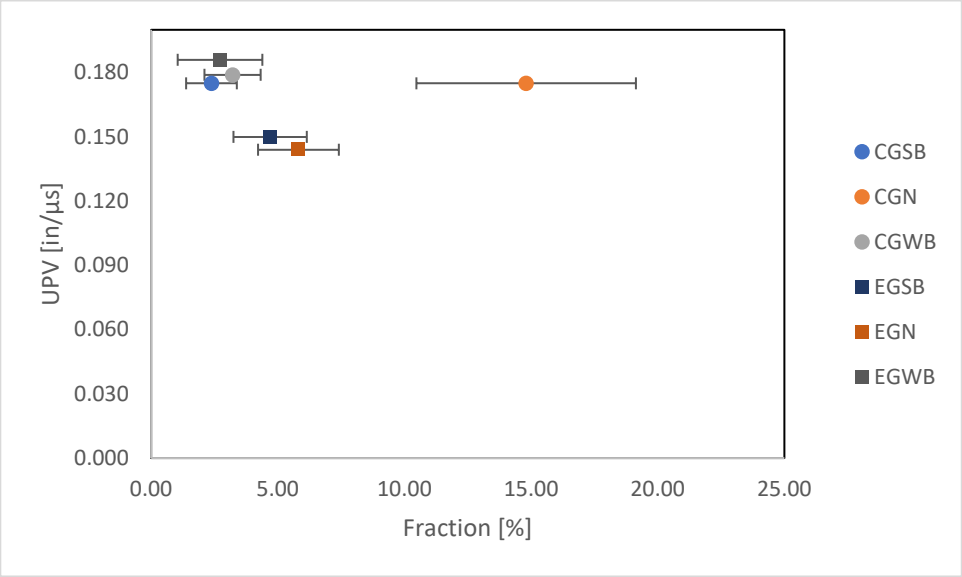

Figure 36. Correlation between UPV and Porosity at 100-µm

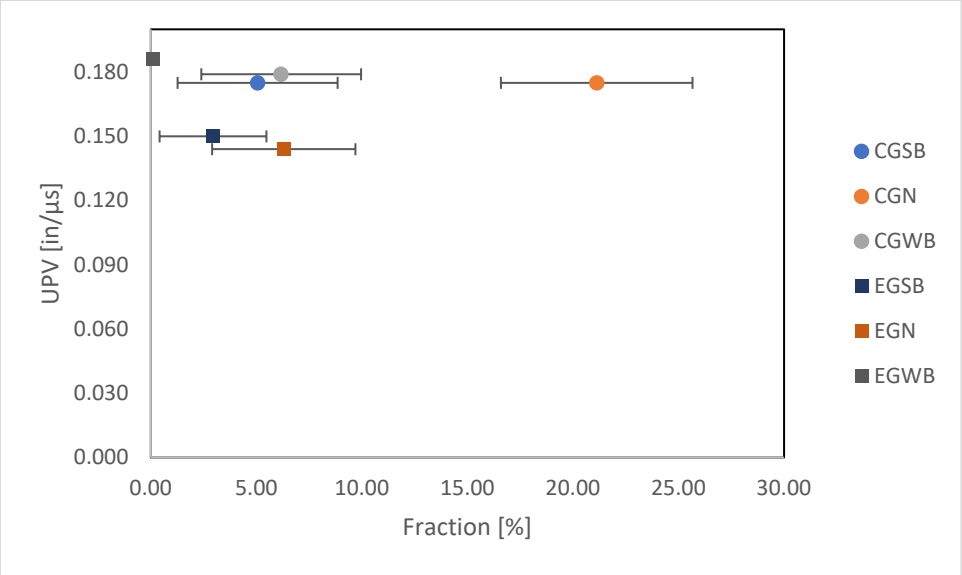

Figure 37. Correlation between UPV and Porosity at 10-µm

The averaged UPV values of the concrete epoxy grout interface specimens supports others' findings that UPV decreases with increasing porosity. This goes in agreement to the conclusion made by Yaman et al. (Yaman et al., 2002). Water blasted and sand blasted cementitious grout likewise supported this trend. It appears that this trend may only apply for low values of porosity; the trendline describing UPV and porosity would interect the x-axis at approximately 8%. This also indicates that, the type of interface preparation technique influences the UPV and porosity values.

Alternatively, for the concrete cementitious grout interface specimens, the sand blasted, and no surface preparation had same averaged UPV values, with the no surface preparation exhibiting a much higher measured porosity value than the sand blasted. The water blasted surface preparation had a higher UPV value which corresponds to a low measured porosity value. Though the cementitious grout interface specimens do not provide a good relation between the averaged UPV values and the measured porosity values, it is thought that UPV values increase with low porosity.

1.4 Conclusion

This research activity focuses on the durability of traditionally specified grouts and various surface treatments of concrete substrate by evaluating chloride permeability, tensile bond performances, and interfacial porosity. The following conclusions can be made from this effort:

- For the case of a constitutive material presentation satisfactory resistance to chloride ion permeability, epoxy grout with suggested.
- The epoxy grout exhibited more hydration in the interfaces, thus decreasing porosity and probably increasing the tensile bond strength.

Since pour-back material must be robust, stable, and resistant to chloride permeability, the epoxy grout with sandblasted surface preparation have proven to meet these criteria by the findings of this experimental work.

RECOMMENDATIONS FOR IMPLEMENTATION

Two grout materials and three types of surface preparation techniques were assessed for their performance as durable PT pour-back materials. After performing laboratory tests, the following recommendations are made.

- Epoxy grout pour-back is highly recommended for dimensional stability.
- Since temperature is associated with the performance of the constitutive material, it is recommended to verify the manufacturer's temperature data and consider ambient conditions preceding to casting pour-backs.
- Great abrasive technique at the interface such as the wet-sand blasting surface preparation at a 3,000-psi pressure.

During the microstructural analysis study, it was observed that the porosity values increased away from the concrete-grout interface specimens. Further studies are needed to investigate the reasons of this happening in the epoxy grout. The role of concrete moisture state on epoxy grout uptake should also be studied. Enhancements to specifications practices could be developed by studying the performance of pour-backs when batched with fibers.

BIBLIOGRAPHY

1. ACI Committee 222. (2001). 222.2 R-01: *Corrosion of Prestressing Steels*. American Concrete Institute.

2. ACI Committee 228-Nondestructive Testing of Concrete. (1998). *Nondestructive Test Methods for Evaluation of Concrete in Structures*. American Concrete Institute.

3. Angst, U., Elsener, B., Larsen, C. K., & Vennesland, Ø. (2009). Critical chloride content in reinforced concrete—A review. *Cement and Concrete Research*, *39*(12), 1122–1138. https://doi.org/10.1016/j.cemconres.2009.08.006

4. ASTM. ASTM C1583: (n.d.). *Test Method for Tensile Strength of Concrete Surfaces and the Bond Strength or Tensile Strength of Concrete Repair and Overlay Materials by Direct Tension (Pull-off Method)*. ASTM International. https://doi.org/10.1520/C1583_C1583M-13

5. *ASTM. ASTM C1556. Test Method for Determining the Apparent Chloride Diffusion Coefficient of Cementitious Mixtures by Bulk Diffusion [Internet]. ASTM International; [cited 2023 Jul 30]. Available from: http://www.astm.org/cgi-bin/resolver.cgi?C1556-11AR16*

6. *ASTM. ASTM C1152. Test Method for Acid-Soluble Chloride in Mortar and Concrete [Internet]. ASTM International; [cited 2023 Jul 30]. Available from: http://www.astm.org/cgi-bin/resolver.cgi?C1152C1152M-04R12E1*

7. Beyene, M. A., Munoz, J. F., Meininger, R. C., & Di Bella, C. (2017). Effect of Internal Curing as Mitigation to Minimize Alkali-Silica Reaction Damage. *ACI Materials Journal*, *114*(3). https://doi.org/10.14359/51689562

8. Bolzoni, F., Brenna, A., & Ormellese, M. (2022). Recent advances in the use of inhibitors to prevent chloride-induced corrosion in reinforced concrete. *Cement and Concrete Research*, *154*, 106719. https://doi.org/10.1016/j.cemconres.2022.106719

9. Burris, L. E., & Riding, K. A. (2014). Diffusivity of Binary and Ternary Concrete Mixture Blends. *ACI Materials Journal*, *111*(4). https://doi.org/10.14359/51686826

10. C09 Committee. (n.d.). *Test Method for Pulse Velocity Through Concrete*. ASTM International. https://doi.org/10.1520/C0597-22

11. Chen, Y., Al-Neshawy, F., & Punkki, J. (2021). Investigation on the effect of entrained air on pore structure in hardened concrete using MIP. *Construction and Building Materials*, *292*, 123441. https://doi.org/10.1016/j.conbuildmat.2021.123441

12. Choinska, M., Khelidj, A., Chatzigeorgiou, G., & Pijaudier-Cabot, G. (2007). Effects and interactions of temperature and stress-level related damage on permeability of concrete. *Cement and Concrete Research*, *37*(1), 79–88. https://doi.org/10.1016/j.cemconres.2006.09.015

13. De La Varga, I., Muñoz, J. F., Bentz, D. P., Spragg, R. P., Stutzman, P. E., & Graybeal, B. A. (2018). Grout-concrete interface bond performance: Effect of interface moisture on the tensile bond strength and grout microstructure. *Construction and Building Materials*, *170*, 747–756. https://doi.org/10.1016/j.conbuildmat.2018.03.076

14. Elsener, B. (2005). Corrosion rate of steel in concrete—Measurements beyond the Tafel law. *Corrosion Science*, *47*(12), 3019–3033. https://doi.org/10.1016/j.corsci.2005.06.021

15. Elsharief, A., Cohen, M. D., & Olek, J. (2003). Influence of aggregate size, water cement ratio and age on the microstructure of the interfacial transition zone. *Cement and Concrete Research*, *33*(11), 1837–1849. https://doi.org/10.1016/S0008-8846(03)00205-9

16. Ghosh, P. (n.d.). *Computation of diffusion coefficients and prediction of corrosion initiation in concrete structures*.

17. Hartt, W. H. (2018). Effect of Modeling Variables upon Projection of Corrosion-Induced Bridge Post-Tension Tendon Failures. *Corrosion*, *74*(7), 768–775. https://doi.org/10.5006/2710

18. He, R., Ye, H., Ma, H., Fu, C., Jin, X., & Li, Z. (2019). Correlating the chloride diffusion coefficient and pore structure of cement-based materials using modified noncontact electrical resistivity measurement. *Journal of Materials in Civil Engineering*, *31*(3), 1–12. https://doi.org/10.1061/(ASCE)MT.1943-5533.0002616

19. Kearsley, E. P., & Wainwright, P. J. (2001). Porosity and permeability of foamed concrete. *Cement and Concrete Research*, *31*(5), 805–812. https://doi.org/10.1016/S0008-8846(01)00490-2

20. Konečný, P., Lehner, P., Ponikiewski, T., & Miera, P. (2017). Comparison of Chloride Diffusion Coefficient Evaluation Based on Electrochemical Methods. *Procedia Engineering*, *190*, 193–198. https://doi.org/10.1016/j.proeng.2017.05.326

21. Lafhaj, Z., Goueygou, M., Djerbi, A., & Kaczmarek, M. (2006). Correlation between porosity, permeability and ultrasonic parameters of mortar with variable water / cement ratio and water content. *Cement and Concrete Research*, *36*(4), 625–633. https://doi.org/10.1016/j.cemconres.2005.11.009

22. Liam, K. C., Roy, S. K., & North wood, D. O. (1992). Chloride ingress measurements and corrosion potential mapping study of a 24-year-old reinforced concrete jetty structure in a tropical marine environment. *Magazine of Concrete Research*, *44*(160), 205–215. https://doi.org/10.1680/macr.1992.44.160.205

23. Martín-Pérez, B., Zibara, H., Hooton, R. D., & Thomas, M. D. A. (2000). A study of the effect of chloride binding on service life predictions. *Cement and Concrete Research*, *30*(8), 1215–1223. https://doi.org/10.1016/S0008-8846(00)00339-2

24. Miller, E., White, B., Haskins, R., Ebeling, R., & Evans, J. (2017). *An investigation of corrosion mitigation strategies for aging post-tensioned cables*. Information Technology Laboratory (U.S.). https://doi.org/10.21079/11681/21478

25. NordTest. (1997). NT Build 355: Chloride Diffusion Coefficient from Migration Cell Experiments. *NordTest Build*, 1–4.

26. NordTest. (1999). NT Build 492: Concrete, mortar and cement-based repair materials: Chloride migration coefficient from non-steady-state migration experiments. *NordTest Build*, 1–8.

27. *NT build 443_Concrete, hardened_Accelerated chloride penetration_Nordtest Method.pdf*. (n.d.).

28. Sakr, K. (2005). Effect of cement type on the corrosion of reinforcing steel bars exposed to acidic media using electrochemical techniques. *Cement and Concrete Research*, *35*(9), 1820–1826. https://doi.org/10.1016/j.cemconres.2004.10.015

29. Scrivener, K. L., Patel, H. H., Pratt, P. L., & Parrott, L. J. (1986). Analysis of Phases in Cement Paste using Backscattered Electron Images, Methanol Adsorption and Thermogravimetric Analysis. *MRS Proceedings*, *85*, 67. https://doi.org/10.1557/PROC-85-67

30. Song, H.-W., Lee, C.-H., & Ann, K. Y. (2008). Factors influencing chloride transport in concrete structures exposed to marine environments. *Cement and Concrete Composites*, *30*(2), 113–121. https://doi.org/10.1016/j.cemconcomp.2007.09.005

31. State of Ohio Department of Transportation. (2014). *Supplemental Specification 855: Post-tensioning*.

32. Stutzman, P. E., & Clifton, J. R. (n.d.). *SPECIMEN PREPARATION for SCANNING ELECTRON MICROSCOPY*.

33. Tatum, G., Brenkus, N., & Ohio State University. Department of Civil and Environmental Engineering and Geodetic Science. (2021). *Division of Engineering Research On-Call Services Task 7: Durability of Anchorage Pour-backs and Improvements* (FHWA/OH-2021-02). https://rosap.ntl.bts.gov/view/dot/59032

34. Tsakiroglou, C. D., Ioannidis, M. A., Amirtharaj, E., & Vizika, O. (2009). A new approach for the characterization of the pore structure of dual porosity rocks. *Chemical Engineering Science*, *64*(5), 847–859. https://doi.org/10.1016/j.ces.2008.10.046

35. Whitmore, D., & Eng, P. (n.d.). *Mitigating Grouted Post-Tension Strand Corrosion on Bridges*.

36. Yaman, I. O., Hearn, N., & Aktan, H. M. (2002). Active and non-active porosity in concrete Part I: Experimental evidence. *Materials and Structures*, *35*(2), 102–109. https://doi.org/10.1007/BF02482109

APPENDIX A – FULL RESULTS

Compression Strength Testing Results

Table 7. 4x8 Concrete Cylinder Compressive Strength Test Results

Age at Testing	Specimen Number	Compressive stress at failure [psi]	Average f'c, psi	Stdev
28-days	1	6,528	6,831	621.2707
	2	7,546		
	3	6,420		
90-days	1	7,093	7,959	768.1734
	2	8,224		
	3	8,559		

Table 8. 2x2 Grout Cubes Compressive Strength Test Results

Age at Testing	Specimen Number	Compressive stress at failure [psi]	Average f'c, psi	Stdev
Epoxy Grout				
28-days	1	12,199	11,473	667.0055
	2	10,887		
	3	11,334		
Cementitious Grout				
28-days	1	8,656	7,305	1221.506
	2	6,279		
	3	6,979		

Modulus of Elasticity Testing Results

Table 9. 90-Day Modulus of Elasticity Test Results

Specimens	Average MOE (psi.)
1	3,053,725
2	4,054,607
3	2,699,388

Chloride Profiling Full Results

Table 10. Chloride Profiling Full Results

Material	Average Layer Depth, x [mm]	Chloride Content, Cxt [% sample weight]	Initial Chloride Content, Ci [% sample weight]	Calculated Surface Chloride Content, Cs [% Sample Weight]	Apparent Diffusion Coefficient, Da [m^2/s]
Concrete	0.5	0.8802	0.0442	0.7308	5.412E-12
	1.5	0.3712			
	2.5	0.4184			
	3.5	0.3021			
	4.5	0.3370			
	5.5	0.2434			
	6.5	0.1728			
	7.5	0.1677			
Epoxy Grout	0.5	0.0740	0.0030	0.4401	3.280E-14
	1.5	0.0510			
	2.5	0.0538			
	3.5	0.0539			
	4.5	0.0460			
	5.5	0.0445			
	6.5	0.0499			
	7.5	0.0464			
Cementitious Grout	0.5	0.7192	0.0306	0.7219	1.397E-12
	1.5	0.4894			
	2.5	0.1814			
	3.5	0.0290			
	4.5	0.0611			
	5.5	0.0549			
	6.5	0.0090			
	7.5	0.4246			

Table 10. continued

Material	Average Layer Depth, x [mm]	Chloride Content, Cxt [% sample weight]	Initial Chloride Content, Ci [% sample weight]	Calculated Surface Chloride Content, Cs [% Sample Weight]	Apparent Diffusion Coefficient, Da [m^2/s]
EGSB	0.5	0.4258	0.0457	0.4483	4.073E-12
	1.5	0.3736			
	2.5	0.2505			
	3.5	0.1492			
	4.5	0.1406			
	5.5	0.1395			
	6.5	0.1119			
	7.5	0.0815			
EGN	0.5	0.4038	0.0439	0.4401	5.156E-12
	1.5	0.2911			
	2.5	0.2523			
	3.5	0.2220			
	4.5	0.1787			
	5.5	0.1387			
	6.5	0.1259			
	7.5	0.1089			
EGWB	0.5	0.4056	0.0447	0.4401	5.341E-12
	1.5	0.3037			
	2.5	0.2405			
	3.5	0.2291			
	4.5	0.1802			
	5.5	0.1476			
	6.5	0.1269			
	7.5	0.1151			

Table 10. continued

Material	Average Layer Depth, x [mm]	Chloride Content, Cxt [% sample weight]	Initial Chloride Content, Ci [% sample weight]	Calculated Surface Chloride Content, Cs [% Sample Weight]	Apparent Diffusion Coefficient, Da [m^2/s]
CGSB	0.5	1.5582	0.0365	1.6794	1.957E-12
	1.5	1.1091			
	2.5	0.6012			
	3.5	0.2078			
	4.5	0.1214			
	5.5	0.1808			
	6.5	0.0985			
	7.5	0.0962			
CGN	0.5	0.7068	0.0420	0.6522	5.544E-12
	1.5	0.4755			
	2.5	0.3482			
	3.5	0.2845			
	4.5	0.2339			
	5.5	0.2189			
	6.5	0.1759			
	7.5	0.1759			
CGWB	1	0.4668	0.0386	0.5202	4.118E-12
	3	0.2071			
	5	0.1680			
	7	0.0940			

Pull-off Test Full Results

Table 11. Pull-off Test Full Results

Specimen	Test Site Number	Strength (Psi)	Failure Mode
EG-No Surface Preparation	1	> 580.2	No failure occurred (Maxxed out tester, grout resistance)
	2	> 580.2	No failure occurred (Maxxed out tester, grout resistance)
	3	> 580.2	No failure occurred (Maxxed out tester, grout resistance)
	4	> 580.2	No failure occurred (Maxxed out tester, grout resistance)
	5	> 580.2	No failure occurred (Maxxed out tester, grout resistance)
EG-Wet Sand Surface Preparation	1	308.4	Epoxy adhesion
	2	441	Epoxy adhesion
	3	133.3	Epoxy adhesion
	4	218.7	Interface failure in Grout
	5	356.3	Interface failure in Grout
EG-Water Jetting Surface Preparation	1	> 580.2	No failure occurred (Maxxed out tester, grout resistance)
	2	> 580.2	No failure occurred (Maxxed out tester, grout resistance)
	3	> 580.2	No failure occurred (Maxxed out tester, grout resistance)
	4	> 580.2	No failure occurred (Maxxed out tester, grout resistance)
	5	> 580.2	No failure occurred (Maxxed out tester, grout resistance)
CG-No Surface Preparation	1	0	Failed During Coring
	2	0	Failed During Coring
	3	0	Failed During Coring
	4	0	Failed During Coring
	5	0	Failed During Coring
	6	0	Failure in grout > Indicates damage during coring and was hanging
	7	43.6	Interface failure in Grout

Table 11. continued

Specimen	Test Site Number	Strength (Psi)	Failure Mode
CG-Wet Sand Jetting Surface Preparation	1	36.9	Interface failure in Grout
	2	78.6	Interface failure in Grout
	3	110.2	Interface failure in Grout
	4	5.1	Failure in grout -> Indicates damage during coring and was hanging
CG-Water Jetting Surface Preparation	1	119.4	Interface failure in Grout
	2	96.1	Interface failure in Grout
	3	136.5	Interface failure in Grout
	4	249.6	Interface failure in Grout

Table 12. Grout Product Names

Label	Product
Cementitious Grout	BASF Materflow 928
Epoxy Grout	BASF Materflow 648 High-strength High-Flow

Microstructural Analysis Full Results

Table 13. Microstructural Analysis Results of Grout

Material	Distance from Concrete Paste Surface (μm)	Total Porosity (%)
CG-N	10	21.12
	20	20.47
	30	19.50
	40	16.49
	50	14.50
	60	12.97
	70	12.17
	80	10.66
	90	10.11
	100	10.07
CG-S	10	5.06
	20	2.76
	30	2.17
	40	2.01
	50	2.11
	60	2.25
	70	2.32
	80	1.94
	90	1.64
	100	1.55

Table 13. continued

Material	Distance from Concrete Paste Surface (μm)	Total Porosity (%)
CG-W	10	6.18
	20	3.49
	30	3.07
	40	3.32
	50	3.17
	60	2.87
	70	2.61
	80	2.61
	90	2.60
	100	2.23
EG-N	10	6.30
	20	2.56
	30	4.08
	40	5.66
	50	6.86
	60	7.42
	70	7.07
	80	7.50
	90	5.86
	100	4.84

Table 13. continued		
EG-S	10	2.95
	20	1.92
	30	4.41
	40	5.54
	50	5.92
	60	5.78
	70	6.46
	80	5.65
	90	4.37
	100	3.98
EG-W	10	0.12
	20	0.29
	30	1.27
	40	2.62
	50	3.91
	60	4.65
	70	4.58
	80	3.96
	90	3.20
	100	2.59

Table 14. Microstructural Analysis Results of Concrete

Material	Distance from Concrete Paste Surface (μm)	Total Porosity (%)
Concrete	10	17.43991
	10	1.879879
	10	0.843156

APPENDIX B – PROPERTIES OF THE LOW VISCOSITY EPOXY RESIN

MAX 1618 A/B

PHYSICAL PROPERTIES

Density	1.10 g/cc +/- 0.03 grams per cubic centimeter Part A
	0.98 +/- .05 grams per cubic centimeter Part B
	1.09.+/-.03 grams per cubic centimeter Mixed
Pounds per Gallon Mixed	9.07 +/- .02 Pounds Per Gallon
Form and Color	PART A = Clear Liquid Gardner Color Scale <1 (Similar to Glycerin or Pure water)
	PART B = Clear Liquid Gardner Color Scale <1 (Similar to Glycerin or Pure water)
	MIXED = Clear Gardner Color Scale 1-2 (Cured specimen 50 grams Mass)
Viscosity	PART A = 980 to 1040 cPs @ 25ºC
	PART B = 300 to 310 cPs @ 25ºC
	MIXED = 337 to 420 cPs @ 25ºC
Mix Ratio	100 Parts "A" to 50 Parts "B" By Weight Or 2:1 By Volume
Working Time	30 Minutes @ 25ºC (300 gram mass)
Peak Exotherm Temperature	174ºC (300-gram concentrated mass) after 50 minutes
Handle Time	6 – 8 Hours Set to Touch, 10 Hours Green Strength
Maximum Operating Temperature	95ºC
Glass Transition	105ºC
Full Cure Time	36 Hrs. Minimum @ 25ºC

Accelerated Cure Schedule	4 hours at 25ºC or until dry to the touch plus 60 Minutes @ 110ºC
Mechanical Properties	
Hardness	87 +/- 5 Shore D
Tee-Peel Strength	5.7 Lbs Per Inch Width Polycarbonate
Tensile Shear Strength	2,300 psi @ 25°C (77°F)
6063 T4 Aluminum	1,800 psi @ -80°C (-112°F)
Overlap Shear	550 psi @ 100°C (212°F)
Elongation	6.0% @ 25°C (77°F)
Flexural Strength	13,500 psi @ 25°C (77°F)
Flexural Modulus	500 psi @ 25°C (77°F)
Compressive Strength	8,200 psi @ 25°C (77°F)
Heat Distortion Temp	80°C (176°F)